A Survey on Protograph LDPC Codes and Their Applications

Yi Fang, Guoan Bi, Yong Liang Guan, and Francis C. M. Lau

***Abstract*—Low-density parity-check (LDPC) codes have attracted much attention in the past two decades since they can asymptotically approach the Shannon capacity in a variety of data transmission and storage scenarios. As a type of promising structured LDPC codes, the protograph LDPC codes not only inherit the advantage of conventional LDPC codes, i.e., excellent error performance, but also possess simple representations to realize fast encoding and efficient decoding. This paper provides a comprehensive survey on the state-of-the-art in protograph LDPC code design and analysis for different channel conditions, including the additive white Gaussian noise (AWGN) channels, fading channels, partial response (PR) channels, and Poisson pulse-position modulation (PPM) channels. Moreover, the applications of protograph LDPC codes to joint source-and-channel coding (JSCC) and joint channel-and-physical-layer-network coding (JCPNC) are reviewed and studied. In particular, we focus our attention on the encoding design and assume the decoder is implemented by the belief propagation (BP) algorithm. Hopefully, this survey may facilitate the research in this area.**

***Index Terms*—Asymptotic weight distribution (AWD), decoding threshold, extrinsic information transfer (EXIT), protograph low-density parity-check (LDPC) codes.**

I. Introduction

Reliable and efficient transmission/storage is one of the ultimate design objectives of modern communication/data storage systems. Among the existing techniques, forward error correction (FEC) is a powerful solution to enhance the reliability of data transmission and storage. The idea of FEC is that incorporating some redundancy into the information bits so as to form a codeword. Instead of the original information, the codeword is transmitted to the receiver through a channel. As a result, the information bits can be successfully retrieved if the codeword is appropriately designed [1].

The history of FEC codes can be dated back to six decades ago. In 1948, C. E. Shannon proved that the error-free (EF) transmission can be achieved for every noisy channel by means of FEC codes with any code rate up to the channel capacity (i.e., maximum achievable code rate) [2], which is called as Shannon theory. Thereby, the maximum amount of the incorporated redundancy that is utilized to ensure correct decoding is determined by the channel capacity. Unfortunately, this theory just quantifies the channel capacity, but does not elaborate how to construct the capacity-approaching codes. Since then, many researchers have endeavored to search the capacity-approaching codes but obtained slow progress. The first FEC code, namely Hamming code, was invented in 1950 [3]. Later, a new FEC code, namely low-density parity-check (LDPC) code, was introduced by R. G. Gallager in his doctoral dissertation [4]. However, in the following 35 years, LDPC codes and their variants were nearly neglected and scarcely considered. One notable contribution during that period is the work of R. M. Tanner [5], who has proposed a graphical representation of the LDPC code — Tanner graph.

In 1993, the turbo code, which enables error performance approaching the channel capacity over additive white Gaussian noise (AWGN) channels, was invented by Berrou *et al.* [6]. In the wake of the remarkable success of turbo codes, the LDPC codes have been rediscovered by Mackay *et al.* because of their capacity-approaching performance under the iterative decoding algorithm [7]–[11]. As compared with turbo codes, LDPC codes possess two distinct advantages: low error-floor and fast decoding [11]–[13]. However, the relatively high encoding complexity is one practical weakness of the LDPC codes. To tackle this problem, several methods have been proposed [14]–[16]. Owing to the above-mentioned advantages, a significant amount of effort has been devoted to analyzing and designing the LDPC codes [12]–[29]. In particular, the density evolution (DE) [12], [13] and extrinsic information transfer (EXIT) function [17]–[19], [29] have been considered as two most popular techniques for optimization of LDPC codes. Besides, the iterative decoding algorithm of LDPC codes has been carefully improved so as to obtain a better decoding performance [30]–[33]. Nowadays, LDPC codes have been widely applied in a myriad of communication and data storage systems, e.g., deep-space communication systems [34], [35], wireless communication systems [36], optical communication systems [37], and magnetic recoding systems [38], [39], and have become one of the most intensely investigated areas in channel coding. The tutorial-style articles of LDPC codes can be found in [26], [40]–[44].

Nevertheless, most capacity-approaching LDPC codes are irregular and hence suffer from the drawback of quadratic encoding complexity. Aiming at overcoming this drawback, one type of structured LDPC codes, namely quasi-cyclic (QC) LDPC codes, has been proposed [45]. Besides, a novel class of LDPC code, namely multi-edge-type (MET) LDPC codes, has been introduced by Richardson *et al.* [42], [46]. As a subclass of MET-LDPC codes, the protograph LDPC codes have emerged as a promising coding scheme because of their

Y. Fang is with the School of Information Engineering, Guangdong University of Technology, Guangzhou, China. He was with the School of Electrical and Electronic Engineering, Nanyang Technological University, Singapore (email: fangyi@gdut.edu.cn).

G. Bi, and Y. L. Guan are with School of Electrical and Electronic Engineering, Nanyang Technological University, Singapore (email: {egbi, eylguan}@ntu.edu.sg).

F. C. M. Lau is with the Department of Electronic and Information Engineering, Hong Kong Polytechnic University, Hong Kong (email: encm-lau@polyu.edu.hk).

excellent error performance and low complexities [47]–[52]. Two classical types of protograph codes, namely accumulate-repeat-3-accumulate (AR3A) code and accumulate-repeat-by-4-jagged-accumulate (AR4JA) code, which can realize linear encoding complexity and fast decoding, have been proposed by Jet Propulsion Laboratory [48]–[50]. Employing the concept of generalized LDPC codes [53], other block code constraints such as Hamming codes and recursive systematic convolutional (RSC) codes can be easily inserted into the protographs to replace selected single-parity-check (SPC) nodes (i.e., check nodes (CNs)) and to form powerful generalized protograph LDPC codes (i.e., doped-Tanner codes) [52], [54]–[57]. In order to facilitate the analysis and design of protograph LDPC codes, the protograph EXIT (PEXIT) algorithm and asymptotic weight enumerator have been proposed in [28], [58] and [50]–[52], respectively. Based on the aforementioned analytical tools, protograph LDPC codes that both possess the capacity-approaching decoding thresholds and linear-minimum-distance property have been constructed [48], [50].

Moreover, the rate-compatible protograph (RCP) LDPC codes have been studied for applications of adaptive coding and hybrid automatic repeat request (HARQ) [50], [59]–[62]. Since non-binary LDPC codes not only can outperform their binary counterparts in some cases (e.g., for short/moderate codeword length), but also can be seamlessly combined with high-order modulations [37], [63]–[65], protograph LDPC codes have been extended to the non-binary domain recently [66]–[69]. As a further advancement, the protograph framework has been introduced for convolutional codes [70] so as to form the protograph LDPC convolutional codes [71]–[73], which have certain advantages as compared to protograph LDPC codes without increasing complexity. In addition, some other variants of protograph codes, such as protograph-based raptor-like (PBRL) codes and spatially-coupled protograph-based (SCPB) codes, have been developed [74]–[78]. Aiming at further reducing the implementation complexity, QC-protograph LDPC codes have been proposed by using the circulant-permutation rules [79], [80]. Inspired by the aforementioned superiorities, many research communities have turned their attention to protograph LDPC codes and hence they appear to be a new major direction for FEC codes in the near future.

In this paper, we conduct a general survey of the state-of-the-art in protograph LDPC code design and analysis over a variety of communication systems, as well as their corresponding applications to joint source-and-channel coding (JSCC) and joint channel-and-physical-layer-network coding (JCPNC). Firstly, an overview of the principle and important milestones of protograph codes is presented. Afterwards, the current research achievement in the design of protograph codes over AWGN channels (i.e., AWGN channel is the most fundamental channel model for protograph codes), fading channels, partial response channels, and Poisson pulse-position modulation (PPM) channels is summarized. Besides, the recent applications of such codes to JSCC and JCPNC are presented, and a modified joint finite-length EXIT algorithm is proposed for analyzing protograph-based JCPNC schemes. Unless otherwise stated, we restrict ourselves to the encoding design of binary protograph LDPC codes and their corresponding analyses.

TABLE I
LIST OF ACRONYMS USED IN THIS SURVEY

AR3A	accumulate-repeat-3-accumulate
AR4JA	accumulate-repeat-by-4-jagged-accumulate
ARA/IARA	accumulate-repeat-accumulate/improved ARA
ARAA	accumulate-repeat-accumulate-accumulate
ARQ/HARQ	automatic repeat request/hybrid ARQ
AWD	asymptotic weight distribution
AWGN	additive white Gaussian noise
BCJR	Bahl-Cocke-Jelinek-Raviv
BER	bit error rate
BF	block-fading
BICM	bit-interleaved coded modulation
BICM-ID	BICM with iterative decoding
BP	belief propagation
BPSK	binary-phase-shift-keying
CC	coded cooperation
CN/CND	check node/CN decoder
DE	density evolution
DF	decode-and-forward
EF	error-free
EXIT/PEXIT	extrinsic information transfer/protograph EXIT
FEC	forward error correction
HD	Hamming-doped
ISI	inter-symbol interference
JCPNC	joint channel-and-physical-layer-network coding
JCPND	joint channel-and-physical-layer-network decoding
JSCC	joint source-and-channel coding
LDPC	low-density parity-check
LLR	log-likelihood-ratio
LTE	Long Term Evolution
MET	multi-edge-type
MI	mutual information
MIMO	multiple-input multiple-output
PBRL	protograph-based Raptor-like
PDF	probability density function
PEG	progressive edge-growth
PNC	physical-layer network coding
PPM	pulse-position modulation
PR	partial response
QC	quasi-cyclic
QSF	quasi-static fading
R4JA	repeat-by-4-jagged-accumulate
RA	repeat-accumulate
RC/RCP	rate-compatible/RC protograph
RP/IRP	root-protograph/improved RP
RSC	recursive systematic convolutional
SCPB	spatially-coupled protograph-based
SIMO	single-input multiple-output
SNR	signal-to-noise-ratio
SPC	single-parity-check
TMDR	typical minimum distance ratio
UEP	unequal error protection
VN/VND	variable node/VN decoder
WER	word error rate

The remainder of this paper is organized as follows. In Section II, the background material of LDPC codes as well as the basic principles and historical overview of protograph codes are provided. In Section III, the achievement of protograph codes in AWGN channels is summarized. The development of protograph codes in other types of channels is introduced in Section IV. In Section V, we survey two attractive applications of protograph codes, i.e., protograph-based JSCC and JCPNC. We also propose a novel joint finite-length EXIT algorithm for the protograph-based JCPNC. Finally, the concluding remarks

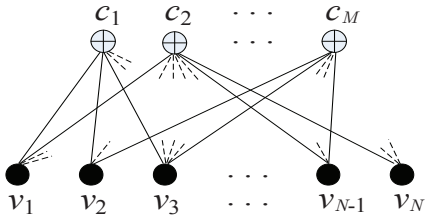

Fig. 1. The Tanner graph of an LDPC code.

and future lines are given in Section VI. The list of acronyms used in this survey is shown in Table I.

II. Principles of Protograph Codes

As a class of outstanding linear block codes, LDPC codes lead the development of modern coding theory because they provide near-capacity performance in a large set of data-transmission and storage channels. In the past fifteen years, more and more sophisticated types of LDPC codes, including protograph codes, have been proposed by the coding community. In this section, the fundamental principles of LDPC codes are reviewed firstly. Afterwards, the protograph codes as well as two corresponding analytical tools are introduced.

A. LDPC Codes

An LDPC code C of length N can be fully represented by a sparse $M \times N$ parity-check matrix $\mathbf{H} = (h_{i,j})$ [4] that has a low density of "1s", where $N - M = K$ denotes the information length, $K/N = R$ denotes the code rate, and $h_{i,j}$ denotes the element in the i-th row and j-th column of $\mathbf{H}$. Moreover, the j-th column and i-th row denote the j-th variable node (VN) v_j and i-th CN c_i, respectively. Hence N and M denote the total numbers of VNs and CNs, respectively. We let $\mathbf{C}_\mu = (v_1, v_2, \ldots, v_N)$ be a specific codeword in C, where $v_j \in \{0, 1\}$. Then we have $\mathbf{C}_\mu \mathbf{H}^{\mathrm{T}} = \mathbf{0}$[1], which is called as the *check-sum constraint*. In the matrix $\mathbf{H}$, the weights of the j-th column and i-th row (denoted by w_{v_j} and w_{c_i}) are defined as the numbers of "1s" in the j-th column and i-th row, respectively, which are also known as the degrees of the j-th VN and i-th CN, respectively (denoted by d_{v_j} and d_{c_i}). The code belongs to *regular* LDPC codes if both the row weight and column weight are constant; otherwise it belongs to *irregular* LDPC codes.

Alternatively, the LDPC code C can be described by an equivalent Tanner graph (i.e., bipartite graph) [5], as shown in Fig. 1. As can be seen from this figure, the VNs and CNs are represented by black circles and circles with a plus sign, respectively, and the edge connecting v_j to c_j corresponds to the element $h_{i,j}$ of $\mathbf{H}$, where $h_{i,j} = 1$. Furthermore, the j-th VN v_j corresponds to the j-th coded bit in C. In a Tanner graph, a cycle is defined as a path starting and ending with the same node without passing through any intermediate nodes more than once. The number of edges in a cycle is termed as the cycle length whereas the shortest cycle length of a Tanner graph is called its girth.

[1]The superscript "T" denotes the transpose operator.

Since the parity-check matrices of LDPC codes possess the sparse property, effective iterative decoding algorithms, such as belief propagation (BP) decoding algorithm [12], [13], can be employed to retrieve the original information from the received signal. To elaborate a little further, we define five types of log-likelihood-ratios (LLRs) as follows.

- $L_{Av}(i, j)$ denotes the input *a-priori* LLR of v_j flowed from c_i on each of the $b_{i,j}$ edges.
- $L_{Ac}(i, j)$ denotes the input *a-priori* LLR of c_i flowed from v_j on each of the $b_{i,j}$ edges.
- $L_{Ev}(i, j)$ denotes the output *extrinsic* LLR sent by v_j to c_i.
- $L_{Ec}(i, j)$ denotes the output *extrinsic* LLR sent by c_i to v_j.
- $L_{app}(j)$ denotes the *a-posteriori* LLR of v_j.

We consider an AWGN channel with binary-phase-shift-keying (BPSK) modulation[2]. The initial LLR (channel message) of the j-th VN v_j is defined as [17]

$$L_{\mathrm{ch},j} = \ln\left[\frac{\Pr(x_j = +1|y_j)}{\Pr(x_j = -1|y_j)}\right] = \frac{2y_j}{\sigma_n^2}, \tag{1}$$

where $\Pr(\cdot)$ denotes the probability function, $y_j = x_j + n_j$ is the channel output, $x_j = (-1)^{v_j} \in \{+1, -1\}$ is the BPSK-modulated bit, and n_j is the Gaussian noise with zero mean and variance $\sigma_n^2 = N_0/2$ (denoted as $n_j \sim \mathcal{N}(0, \sigma_n^2)$). Using the BP decoding algorithm, the reliability of the a-posteriori LLRs $\{L_{app}(j)\}$ of C will be improved via exchanging extrinsic LLRs $\{L_{Ev/Ec}(i, j)\}$ between the VN decoder (VND) and CN decoder (CND) iteratively, where the decoding routing is exactly characterized by the Tanner graph. Interested readers can refer to [12], [13] for more details of the BP decoding algorithm. In the remainder of this paper, we assume that the LDPC codes are decoded by the BP algorithm unless otherwise mentioned[3].

Yet, the above-reported LDPC codes are unstructured and thus require relatively high encoding complexity, which prevents them from being utilized in practice. For this reason, several research attempts have been made to design good structured LDPC codes, e.g., cyclic and QC-LDPC codes [81]. Meanwhile, the MET-LDPC code, which is considered as a type of intermediate code that establishes a bridge between the conventional LDPC codes and the protograph codes, has been proposed [46]. The MET-LDPC codes not only outperform the conventional LDPC codes, but also possess lower encoding complexity. The main idea of such codes is "multi-edge type", which means that there exist multiple edge types in a MET-LDPC code and each type may contain multiple edges. As is well known, all the edges in a conventional LDPC code are interchangeable, meaning that there exists only one edge type. Based on this difference, the conventional LDPC codes can be specified by the degree-distribution pair while the MET-LDPC codes should be specified by both the number of edge types and the number of edges in each type (i.e., edge-connection property).

[2]Unless otherwise stated, we assume that the modulation technique used in this paper is BPSK.

[3]*Note that* the BP decoding algorithm is also suitable for the structured LDPC codes, such as cyclic/QC-LDPC codes and protograph codes, which are subclasses of LDPC codes.

Motivated by the desirable advantages of MET-LDPC codes, protograph codes that exhibit even simpler structure, lower complexity, and better performance, have been further proposed [47] and they provide a new major direction for code construction.

B. Protograph Codes

A protograph, which was first introduced in [47], is a Tanner graph with a relatively small number of nodes. A protograph $\mathcal{G} = (\mathcal{V}, \mathcal{C}, \mathcal{E})$ consists of three sets $\mathcal{V}$, $\mathcal{C}$, and $\mathcal{E}$, respectively, corresponding to $N_{\rm P}$ VNs, $M_{\rm P}$ CNs, and the connecting edges[4]. Each edge $e_{i,j} \in \mathcal{E}$ connects a VN $v_j \in \mathcal{V}$ to a CN $c_i \in \mathcal{C}$. Unlike conventional LDPC codes, parallel edges are allowed in a protograph, i.e., the mapping $e_{i,j} \to (v_j, c_i)$ may not be one-to-one. Furthermore, the code rate is given by $R = (N_{\rm P} - M_{\rm P})/N_{\rm P}$ and the adjacency matrix of a protograph is defined as an $M_{\rm P} \times N_{\rm P}$ *base matrix* $\mathbf{B} = (b_{i,j})$, where $b_{i,j}$ represents the number of edges connecting v_j to c_i. Referring to the leftmost protograph shown in Fig. 2, it consists of 4 VNs, 3 CNs, and 9 edges (i.e., 8 different edge types) and the corresponding base matrix is given by

$$\mathbf{B} = \begin{array}{c} \begin{array}{cccc} v_1 & v_2 & v_3 & v_4 \end{array} \\ \begin{pmatrix} 1 & 1 & 1 & 2 \\ 1 & 1 & 0 & 0 \\ 1 & 0 & 1 & 0 \end{pmatrix} \end{array} \begin{array}{c} c_1 \\ c_2 \\ c_3 \end{array}. \tag{2}$$

As in conventional LDPC codes, the weight of the j-th column (i-th row) in the base matrix $\mathbf{B}$ is defined as the summation of the non-zero elements in this column (row) and it corresponds to the degree of the j-th VN (i-th CN)[5].

A large protograph of size $M \times N$ (where $M = zM_{\rm P}$, $N = zN_{\rm P}$), namely a *derived graph* and corresponding to a protograph code, can be constructed by performing a "copy-and-permute" operation on a given protograph where z represents the number of such operations. The "copy-and-permute" and "z" are also known as "lifting" and "lifting factor", respectively [50]. Consequently, codes of arbitrary lengths can be generated by varying the lifting factor z. In practice, one can exploit a modified version of the progressive-edge-growth (PEG) algorithm [82], [83] to implement the lifting operation. A simple example of generating a derived graph is illustrated in Fig. 2. Referring to this figure, a derived graph is constructed by copying the protograph 2 times and permuting the edges that belong to the same type. The LDPC code corresponding to the resultant derived graph is defined as a protograph code.

Actually, a lot of conventional LDPC codes can be generated by means of protographs, e.g., the repeat-accumulate (RA) code and the regular LDPC code [48]. As two typical families of protograph codes, the AR3A code and the AR4JA code, which possess excellent performance in the low-SNR region and high-SNR region, respectively, over AWGN channels, have been proposed in [48]–[50]. Both codes have very simple protograph representations that enable linear encoding complexity as well as fast decoding. The structures of the AR3A code and AR4JA code with a code rate $R = (n+1)/(n+2)$ $(n = 0, 1, \ldots)$ are shown in Fig. 3, where blank circles denote punctured VNs[6]. In fact, many existing protograph codes involve untransmitted (i.e., punctured) VNs which can yield an increase in code rate and an improvement in decoding threshold. These VNs are decoded by the decoder in the same way as if the channel has an "erasure". In this paper, we define P_j as the *punctured label* of v_j, where $P_j = 0$ if v_j is punctured and $P_j = 1$ otherwise.

C. PEXIT Algorithm

Among the existing techniques introduced for the convergence analysis of iterative processors [12], [13], [17]–[19], [85], the EXIT function [17]–[19] attains large attention because of its simplicity and accuracy. The EXIT function is very useful in tracing the convergence of the iterative processors used in a variety of communication problems, such as the iterative decoders in communication systems. To be specific, the EXIT chart, which describes the asymptotic decoding trajectory of a decoder, consists of two EXIT curves. The decoder will converge successfully if the two EXIT curves do not touch or cross each other except at the value of unity. Using this tool, one can derive the decoding threshold[7] and predict the asymptotic error performance of a (concatenated) code under a given iterative decoder. Although the infinite-length EXIT chart is an asymptotically analytical method, it provides a nice way to predict the performance for the cases of finite codeword length. In order to overcome the weakness of EXIT chart and to make a more accurate prediction for the convergence performance of the short/moderate codeword length, some finite-length analytical techniques, including the finite-length EXIT algorithm, have been proposed [86]–[88].

Since the discovery of protograph codes by J. Thorpe in 2003 [47], much attention has been turned to this type of codes. Nevertheless, most designs and analyses of the codes have relied on the DE[8] due to the fact that the conventional EXIT algorithm [17], [18] is not applicable to protograph codes. The main reasons that prevent the usage of conventional EXIT algorithm are shown as below.

1) Degree-1 VNs and punctured VNs may exist in the protograph codes. However, the conventional EXIT algorithm is described based on the degree-distribution pair of LDPC

[4]For simplicity of description, we define $M_{\rm P} \times N_{\rm P}$ as the size of the protograph.

[5]More precisely, the degree of a VN (CN) is defined as the number of the edges connected to this VN (CN) in the protograph.

[6]In coding theory, puncturing is the process of removing some of the parity bits from the codeword after encoding. At the beginning, this technique was proposed for increasing the code rate [84]. Yet, it has been pointed out that the decoding threshold can also be improved if the punctured VNs are appropriately selected, especially for protograph codes [49], [50].

[7]For a given channel and a given iterative decoder, the decoding threshold of a code, i.e., $(E_b/N_0)_{\rm th}$, is defined as the signal-to-noise-ratio (SNR) above which an arbitrarily small bit error rate (BER) can be achieved as the codeword length approaches infinity. Shannon capacity is considered as the fundamental lower-limit on $(E_b/N_0)_{\rm th}$ of any coding scheme with a code rate R. As a consequence, $(E_b/N_0)_{\rm th}$ is always larger than Shannon capacity.

[8]As a general tool for analyzing LDPC codes, DE was firstly proposed by Richardson *et al.* [12], [13] and has been widely utilized in LDPC-code design. The principle of this technique is to trace the evolution of the LLR distribution in the iterative decoder so as to determine the decoding threshold of a code.

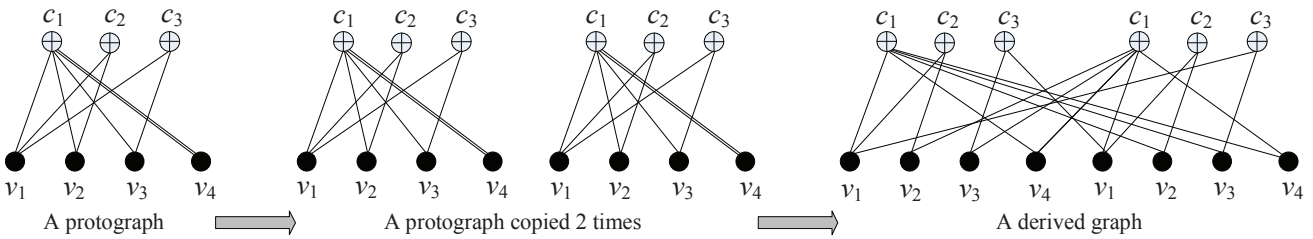

Fig. 2. A simple example of generating the derived graph.

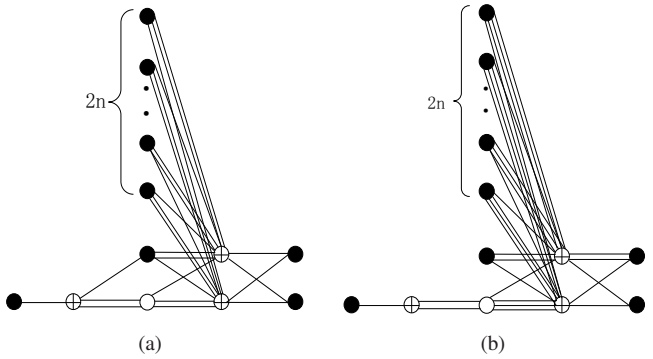

Fig. 3. The protographs of (a) an AR3A code and (b) an AR4JA code.

codes, in which degree-1 VNs are not allowed and punctured VNs cannot be identified. Hence, the corresponding decoding threshold provided by such an EXIT algorithm is not precise.

2) Some protograph codes may share the same degree-distribution pair but have different protograph representations (i.e., base matrices). For this scenario, the protograph codes should exhibit different convergence behaviors. Yet, the conventional EXIT algorithm cannot distinguish the difference among these codes.

As a result, taking into consideration the different edge-connection properties, the PEXIT algorithm has been proposed by Liva *et al.* [28], [58], in which the mutual information (MI) [89] is calculated for each VN and CN rather than degree-distribution pair. The introduction of PEXIT algorithm reduces the complexity of the related design work in comparison with that of DE. We now briefly review this important algorithm. For the ease of description, we first define five types of MI for the protograph codes.

- $I_{Av}(i,j)$ denotes the *a-priori* MI between $L_{Av}(i,j)$ and the corresponding coded bit v_j.
- $I_{Ac}(i,j)$ denotes the *a-priori* MI between $L_{Ac}(i,j)$ and the corresponding coded bit v_j.
- $I_{Ev}(i,j)$ denotes the *extrinsic* MI between $L_{Ev}(i,j)$ and the corresponding coded bit v_j.
- $I_{Ec}(i,j)$ denotes the *extrinsic* MI between $L_{Ec}(i,j)$ and the corresponding coded bit v_j.
- $I_{app}(j)$ denotes the *a-posteriori* MI between $L_{app}(j)$ and the corresponding coded bit v_j.

The block diagram of the PEXIT algorithm is depicted in Fig. 4. As can be seen, the output extrinsic MI of one decoder becomes the input a-priori MI of the other decoder during each iteration, i.e., $I_{Ac}(i,j) = I_{Ev}(i,j)$ and $I_{Av}(i,j) = I_{Ec}(i,j)$.

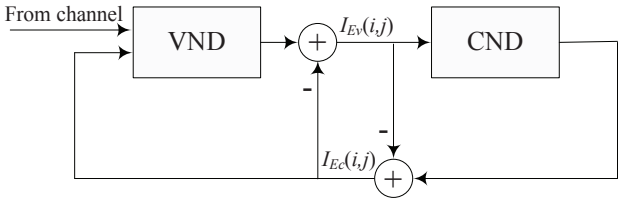

Fig. 4. Block diagram of the PEXIT algorithm.

The **PEXIT algorithm** in an AWGN channel is described as follows.

1) For $i = 1, 2, \ldots, M_{\mathrm{P}}$ and $j = 1, 2, \ldots, N_{\mathrm{P}}$, initialize $I_{Av}(i,j) = 0$. Then, compute the variance of the channel initial LLR as $\sigma^2_{\mathrm{ch},j} = 8P_j(E_s/N_0) = 8P_jR(E_b/N_0)$, where R is the code rate, E_s/N_0 is the SNR per symbol, $E_b/N_0 = (E_s/N_0)/R$ is the SNR per bit, and P_j is the *punctured label* of v_j (i.e., $P_j = 0$ if v_j is punctured and $P_j = 1$ otherwise).
2) For $i = 1, 2, \ldots, M_{\mathrm{P}}$ and $j = 1, 2, \ldots, N_{\mathrm{P}}$, calculate the output extrinsic MI $I_{Ev}(i,j)$ sent by v_j to c_i if $b_{i,j} \neq 0$ using [28, eq.(11)], which is given as (3) at the top of the following page. Here, $J(\cdot)$ function and its inverse function $J^{-1}(\cdot)$ are defined in [18].
3) For $i = 1, 2, \ldots, M_{\mathrm{P}}$ and $j = 1, 2, \ldots, N_{\mathrm{P}}$, measure the output extrinsic MI $I_{Ec}(i,j)$ sent by c_i to v_j if $b_{i,j} \neq 0$ exploiting [28, eq.(12)], which is shown as (4) at the top of the following page.
4) For $j = 1, 2, \ldots, N_{\mathrm{P}}$, compute the a-posteriori MI of v_j as

$$I_{app}(j) = J\left(\sqrt{\left(\sum_{i=1}^{M_{\mathrm{P}}} b_{i,j}[J^{-1}(I_{Av}(i,j))]^2\right) + \sigma^2_{\mathrm{ch},j}}\right). \tag{5}$$

5) If the a-posteriori MI values $I_{app}(j) = 1$ for all $j = 1, 2, \ldots, N_{\mathrm{P}}$, the E_b/N_0 value is output as the decoding threshold and the iterative process is stopped; otherwise, we go to Step 2 to continue the iterative process.

Table II lists the decoding thresholds $(E_b/N_0)_{\mathrm{th}}$ (dB) of the AR4JA code with different code rates obtained by the DE and PEXIT methods, as well as the gaps between them. The results suggest that the PEXIT algorithm can provide an accurate evaluation of the decoding threshold for all code rates, with a difference no larger than 0.005 dB compared to the ones found by DE. In summary, the PEXIT algorithm reduces much computational complexity in calculating the decoding threshold as compared to the DE without sacrificing the accuracy. In the remainder of this paper, we will calculate

$$I_{Ev}(i,j) = J\left(\sqrt{\left(\sum_{\mu\neq i} b_{\mu,j}[J^{-1}(I_{Av}(\mu,j))]^2\right) + (b_{i,j}-1)[J^{-1}(I_{Av}(i,j))]^2 + \sigma_{\mathrm{ch},j}^2}\right) \tag{3}$$

$$I_{Ec}(i,j) = 1 - J\left(\sqrt{\left(\sum_{\mu\neq j} b_{i,\mu}[J^{-1}(1-I_{Ac}(i,\mu))]^2\right) + (b_{i,j}-1)[J^{-1}(1-I_{Ac}(i,j))]^2}\right) \tag{4}$$

TABLE II
DECODING THRESHOLDS $(E_b/N_0)_{\mathrm{th}}$ (dB) OF THE AR4JA CODE WITH DIFFERENT CODE RATES CALCULATED BY THE DE AND PEXIT METHODS, AS WELL AS THE GAPS $|\epsilon|$ BETWEEN THEM.

R	1/2	2/3	3/4	4/5	5/6	6/7	7/8
DE	0.628	1.450	2.005	2.413	2.733	2.993	3.209
PEXIT	0.623	1.455	2.003	2.411	2.730	2.990	3.207
$\lvert\epsilon\rvert$	0.005	0.005	0.002	0.002	0.003	0.003	0.002

TABLE III
DECODING THRESHOLDS $(E_b/N_0)_{\mathrm{th}}$ (dB) AND TMDRS $\delta_{\min}$ OF THE RATE-1/2 $(3,6)$ REGULAR PROTOGRAPH CODE, PRECODED $(3,6)$ REGULAR PROTOGRAPH CODE, AR3A CODE, AND AR4JA CODE IN AN AWGN CHANNEL.

Code Type	Regular	Precoded	AR3A	AR4JA
$(E_b/N_0)_{\mathrm{th}}$	1.103	0.869	0.478	0.623
$\delta_{\min}$	0.023	0.028	none	0.014

the decoding thresholds of all protograph codes using the PEXIT algorithm.

D. Asymptotic Weight Distribution (AWD)

The PEXIT algorithm is served as an important theoretical tool to design the protograph codes with capacity-approaching decoding threshold. However, the decoding threshold is unable to characterize a protograph code completely, especially for the error performance in the high-SNR region. The protograph codes having capacity-approaching threshold may exhibit good performance in the low-SNR region but suffer from an abrupt decrease in the slope of the error-rate curve, called as *error floor*, in the high-SNR region [25], [90]. Error floor is a common phenomenon for LDPC codes and it is mainly attributed to the sub-optimality of iterative decoding algorithms (e.g., BP decoding algorithm) on the Tanner graphs with cycles. In [91], [92], the authors have found that error performance in the high-SNR region and the error-floor phenomenon can be characterized by the minimum (Hamming) distance of the code. Furthermore, it has been pointed out that LDPC codes that have minimum distance growing linearly with the codeword length (i.e., linear-minimum-distance property) possess a relatively lower error floor as compared with their counterparts that do not show such a property [91]–[93].

Motivated by the above-mentioned discussions, the AWD analysis, which can be used to evaluate the minimum distance of protograph codes, has been proposed and used in [48], [50]–[52], [94] so as to complement the PEXIT algorithm. According to [48], [50], the normalized logarithmic AWD function of a protograph ensemble can be expressed as

$$r(\delta) = \max_{\boldsymbol{\delta}_{\mathrm{t}}:|\boldsymbol{\delta}_{\mathrm{t}}|=N_{\mathrm{t}}\delta} \left\{ \sum_{i=1}^{M_{\mathrm{P}}} \phi^{c_i}(\boldsymbol{\delta}_i) - \sum_{j=1}^{N_{\mathrm{P}}} (d_{v_j}-1) H(\delta_j) \right\} \Big/ N_{\mathrm{t}} \ , \tag{6}$$

where δ denotes the normalized weight of the protograph code; M_{P}, N_{P}, and N_{t} respectively denote the numbers of the CNs, VNs, and transmitted VNs; d_{v_j} denotes the degree of the VN v_j; $\boldsymbol{\delta}_{\mathrm{t}} = (\delta_1, \delta_2, \ldots, \delta_{N_{\mathrm{t}}})$ and $\boldsymbol{\delta}_i = (\delta_{i,1}, \delta_{i,2}, \ldots, \delta_{d_{c_i}})$ denote the vectors of normalized partial weights of the transmitted VNs and the VNs associated with a degree-d_{c_i} CN, respectively, where $0 \leq \delta_j \leq 1$; $\phi^{c_i}(\boldsymbol{\delta}_i)$ is the normalized logarithmic AWD for the CN c_i; and $H(x)$ is the binary entropy function [89]. Specifically, the normalized logarithmic AWD for a degree-3 CN c_i is given as $\phi^{c_i}(\boldsymbol{\delta}_i) = \phi^{c_i}(\delta_{i1}, \delta_{i2}, \delta_{i3}) = H_4(\vartheta - \delta_{i1}, \vartheta - \delta_{i2}, \vartheta - \delta_{i3}, 1 - \vartheta)$, where $\vartheta = (\delta_{i1} + \delta_{i2} + \delta_{i3})/2$, $H_4(x_1, x_2, x_3, x_4) = -\sum_{\mu=1}^{4} x_\mu \ln x_\mu$, and $\max\{\delta_{i1}, \delta_{i2}, \delta_{i3}\} \leq \vartheta \leq 1$. The normalized logarithmic AWD for a higher-degree ($d_{c_i} > 3$) CN can also be obtained by using a CN-splitting technique [50].

Exploiting the AWD analysis, one can identify whether the minimum distance $d_{\min}$ of a protograph ensemble increases linearly with the codeword length N or not. If the function $r(\delta)$ starts from zero and goes to negative before crossing zero again at $\delta = \delta_{\min} > 0$, then $d_{\min}$ increases linearly with N at the rate $\delta_{\min}$ with a high probability. In other words, $\Pr(d_{\min} = \delta_{\min} N) = 1 - \zeta$ for any $0 < \zeta < 1$. The rate $\delta_{\min}$, which describes the characteristic of the minimum distance of a protograph ensemble, is defined as the *typical minimum distance ratio* (TMDR). More details of the AWD analysis can be referred to [48], [50]–[52], [94].

As an example, we derive and plot the AWD of the rate-$1/2$ AR3A code and AR4JA code in Fig. 5. For comparison, we also consider the AWD of the rate-$1/2$ $(3,6)$ regular protograph code, precoded $(3,6)$ regular protograph code [48], and random code in the same figure. We observe that the AR4JA code, regular protograph code, precoded protograph code, and random code possess the TMDRs, while the AR3A code does not have the TMDR. It implies that the minimum distance of the AR3A code does not increase linearly with the codeword length and hence an error floor may appear in the high-SNR region. Among the four codes that possess the linear-minimum-distance property, the TMDR of random code is the largest. However, random codes are impractical.

In Table III, we further compare the decoding thresholds

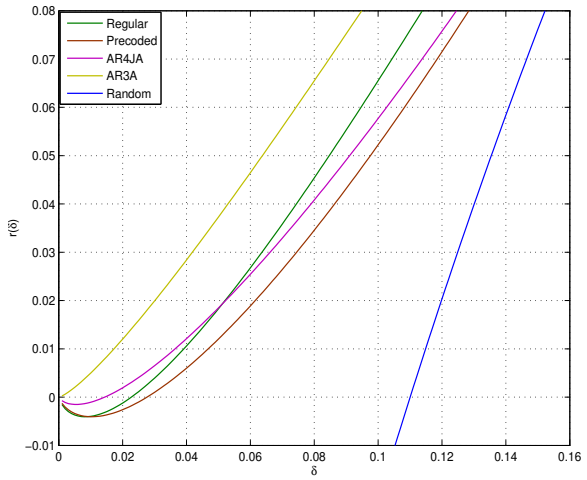

Fig. 5. AWD curves of the rate-$1/2$ $(3, 6)$ regular protograph code, precoded $(3, 6)$ regular protograph code, AR3A code, AR4JA code, and random code.

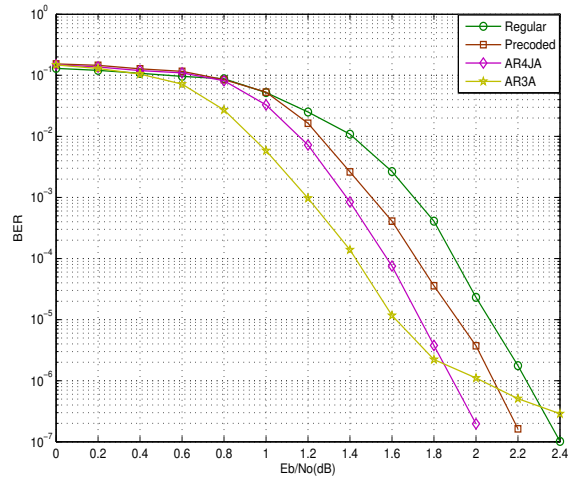

Fig. 6. BER curves of the rate-$1/2$ $(3, 6)$ regular protograph code, precoded $(3, 6)$ regular protograph code, AR3A code, and AR4JA code with information length $K = 1024$ in an AWGN channel.

and TMDRs of the four decodable rate-$1/2$ protograph codes in an AWGN channel. Referring to this table, the AR3A code, which cannot achieve the linear minimum distance, has the lowest threshold. Consequently, the AR3A code should perform best in the low-SNR region but may be outperformed by other codes in the high-SNR region, especially for short codeword lengths. On the contrary, the AR4JA code not only possesses the second-lowest threshold but also exhibits the linear-minimum-distance property and thus may provide excellent error performance in both the low and high-SNR regions. Fig. 6 plots the BER curves of the four decodable rate-$1/2$ protograph codes with information length $K = 1024$ in an AWGN channel using the BP decoding algorithm [12], [13]. The results are highly consistent with the aforementioned analyses.

Note also that

- The PEXIT algorithm is related to both the code and the channel.
- The AWD is dependent on the type of code, but independent of the type of channel.

E. Historical Development of Protograph Codes

Based on the PEXIT algorithm and AWD, many contributions related to the design and analysis of protograph codes as well as their variants have been achieved for a variety of channel conditions [59]–[62], [66]–[80], [83], [88], [94]–[116]. Furthermore, the applications of protograph codes to other areas beyond channel coding, such as JSCC and JCPNC, have been extensively investigated [117]–[123]. The major contributions on the study of protograph codes in the past twelve years are summarized in Table IV.

F. Conclusions

In this section, we have briefly reviewed the basic principles of LDPC and protograph codes, including their definitions, representation methods, and the BP decoding algorithm. We have also introduced two fundamental analytical tools, i.e., PEXIT algorithm and AWD, which are of great importance to design capacity-approaching protograph codes with linear-minimum-distance property. Following these preliminary foundations, a brief historical overview of protograph codes has also been provided.

III. Design of Protograph Codes in AWGN Channels

Initially, the protograph codes were proposed for deep-space communication systems, which can be modeled as a nearly perfect AWGN channel [47], [124]. As a consequence, a significant amount of work has been endeavored to investigate such codes in AWGN channels. In this section, we first describe the properties for a good protograph code. Subsequently, the design of the fixed-rate protograph codes and RCP codes that possess capacity-approaching thresholds and linear minimum distance is introduced. Finally, the construction method of bilayer protograph codes for relay systems is presented.

A. Properties of a Good Protograph Code

According to the discussions in Sect. II and [48]–[52], [61], [94]–[96], the properties of a good protograph code can be concluded as follows.

1) Capacity-approaching decoding threshold: The near-capacity decoding threshold, which can be realized by including at least one high-degree VN and a proper proportion of degree-2 VNs [12], [49]–[52], is one of the ultimate objectives for the design of protograph codes.

2) Linear minimum distance: Linear minimum distance is another desirable property of good LDPC codes and can be used to predict the error-floor behavior for finite-length codewords. The linear-minimum-distance property of the protograph codes, which is sensitive to the proportion of degree-2 VNs, can be determined by the AWD analysis [48], [50]. In [51], the authors have proposed a particular class of protograph codes with a proper proportion of degree-2 VNs so as to ensure this property.

TABLE IV
MAJOR CONTRIBUTIONS ON STUDYING PROTOGRAPH CODES.

Year	Author(s)	Contribution
2002	Richardson *et al.* [46]	Introduced MET-LDPC codes, i.e., a generalization of the regular and irregular LDPC codes.
2003	J. Thorpe [47]	Proposed the fundamental framework of protograph codes.
2004	Abbasfar *et al.* [98]	Proposed the protograph-based RA codes, irregular RA codes, and accumulate-RA (ARA) codes. In particular, proposed the AR3A code, which provides fast encoding structure and low decoding threshold.
2004	Divsalar *et al.* [99]	Proposed a new protograph coding scheme based on ARA codes, called accumulate-repeat-accumulate-accumulate (ARAA) codes, which also realize efficient encoding and low decoding thresholds.
2005	Divsalar *et al.* [100]	Extended the construction of ARA codes to low code rates $(R < 1/2)$, which retain the low decoding thresholds close to the channel capacity.
2005	Divsalar *et al.* [48]	Proposed the AWD analysis for protograph codes. Further, proposed several code constructions that simultaneously accomplish low threshold and linear minimum distance.
2006	Abu-Surra *et al.* [54]–[56]	Designed doped-Tanner codes, i.e., generalized protograph codes, by inserting powerful block code constraints into protographs, which lead to the lower error floors as compared with the existing protograph codes.
2006	Liva *et al.* [28]	Invented the PEXIT algorithm, which provides an efficient way to evaluate the decoding threshold of protograph codes.
2007	Abbasfar *et al.* [49]	Analyzed the performance of ARA codes with maximum-likelihood decoding and derived the weight distribution of them.
2007	Abu-Surra *et al.* [97]	Calculated the AWD and stopping set enumerators for the generalized protograph codes.
2007	Liva *et al.* [57]	Presented a novel methodology for designing the QC-generalized protograph codes, which lead to the outstanding performance in both the waterfall region and error-floor region.
2008	Bonello *et al.* [79]	Proposed the QC-protograph codes based on Vandermonde matrices, which further reduce the implementation complexity without any compromise in the attainable error performance.
2008	Mitchell *et al.* [71], [72]	Proposed the protograph-based convolutional codes and derived a lower-bound on the free distance of this type of codes.
2009	Divsalar *et al.* [50]	Proposed the construction methodologies to design protograph codes that achieve both capacity-approaching thresholds and linear minimum distance, as well as offered the implementation of high-throughput BP decoder.
2010	Abu-Surra *et al.* [51]	Proved that the TMDR exists for a certain class of protograph codes with degree-2 VNs.
2010	Butler *et al.* [95]	Developed and evaluated the upper-bounds on the (Hamming) distance of QC-protograph codes, e.g., the QC-AR4JA code.
2011	Yang *et al.* [83]	First application and performance evaluation of protograph codes in PR channels.
2011	Nguyen *et al.* [106]	Proposed a method to design the protograph-based bit-interleaved coded modulation (BICM) in Rayleigh fading channels.
2011	Chen *et al.* [75]	Presented a new class of RC-LDPC codes based on protograph structures, i.e., PBRL codes.
2011	Uchikawa *et al.* [77]	First introduction and performance evaluation of the SCPB codes.
2011	Chang *et al.* [66]	First extension of protograph codes to the non-binary domain so as to form non-binary protograph codes.
2012	Nguyen *et al.* [61]	Proposed an approach for constructing capacity-approaching RCP codes with a wide range of code rates.
2012	Fang *et al.* [88]	Proposed a finite-length EXIT analysis and a two-step design methodology for protograph codes in PR channels.
2012	Iyengar *et al.* [105]	Developed a windowed decoding algorithm for the protograph-based convolutional codes in erasure channels.
2012	Fang *et al.* [107]	Extended the PEXIT algorithm for protograph codes to ergodic fading channels.
2012	Pulini *et al.* [109]	Extended the PEXIT algorithm for protograph codes to non-ergodic block-fading (BF) channels.
2012	Chen *et al.* [121]	First application of protograph codes to JCPNC systems.
2012	He *et al.* [117]	First application of protograph codes to JSCC systems.
2013	Mitchell *et al.* [73]	Analyzed the minimum distance and trapping set of the protograph-based convolutional codes.
2013	C. A. Kelley [104]	Proposed the algebraic protograph codes and their corresponding implementation.
2013	Nguyen *et al.* [102]	Proposed a simple approach for constructing bilayer protograph codes so as to obtain excellent performance in AWGN half-duplex relay channels.
2013	Fang *et al.* [108]	Analyzed the asymptotic error-performance of protograph codes in ergodic fading channels.
2013	Fang *et al.* [123]	Proposed the performance analysis and precoding design for protograph-based JCPNC schemes in ergodic fading channels.
2013	Zhou *et al.* [103]	Optimized the protograph-based BICM with iterative-decoding (BICM-ID) in Poisson PPM channels.
2014	Dolecek *et al.* [69]	Provided a comprehensive analysis and design of non-binary protograph codes.
2014	Fang *et al.* [111], [112]	Designed the full-diversity root-protograph (RP) and RCRP codes for the point-to-point BF and relay BF channels, respectively.
2014	Wu *et al.* [120]	Proposed a joint PEXIT algorithm for protograph-based JSCC schemes in ergodic fading channels.

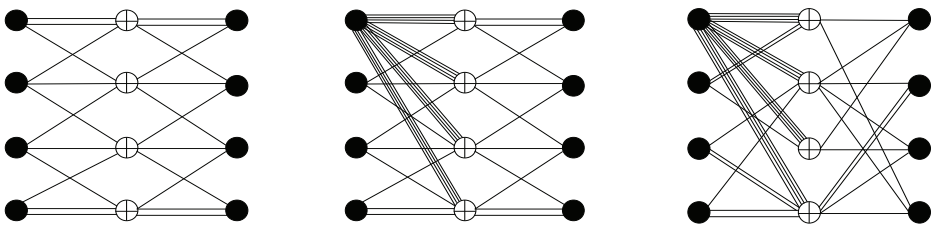

(a) (b) (c)

Fig. 7. The protographs of (a) a rate-$1/2$ $(3, 6)$ regular protograph code, (b) a protograph code with a high-degree VN, and (c) an optimized protograph code with VN degrees at least 3.

3) Precoding structure: In a protograph, the precoding structure is defined as a rate-1 accumulator that contains a degree-1 VN, a higher-degree punctured VN, and a CN that connects the former two VNs [48], [49]. Using precoding structure can always lower the decoding threshold and increase the linear minimum distance (i.e., TMDR) of a protograph code, such as the precoded $(3, 6)$ regular protograph code and the AR4JA code.

To summarize, a punctured protograph code which satisfies the above-mentioned three properties should provide excellent error performance in AWGN channels while a good unpunctured protograph code only needs to possess the former two properties.

B. Design of Fixed-Rate Protograph Codes

In this subsection, we mainly focus on the design of rate-$1/2$ protograph codes. Yet, the results can be easily extended to higher code rates (i.e., $R > 1/2$). For designs of lower-rate (i.e., $R < 1/2$) protograph codes, please refer to [100], in which various low-rate $(R = 1/3, 1/4, \ldots, 1/10)$ AR3A codes and AR4A codes have been proposed.

1) Generalized design scheme: Till now, most contributions related to the design of protograph codes are obtained by using computer-search-based methods under the constraints listed in Sect. III-A. The **generalized design scheme** for the fixed-rate protograph codes is summarized as follows.

(1) Assume the numbers of CNs and VNs in the protograph, and begin the optimization with a reference protograph;
(2) Impose the constraints, which lead to a desirable decoding threshold, on the protograph;
(3) Impose the constraints, which lead to a linear minimum distance, on the protograph;
(4) Add a precoding structure, i.e., a degree-1 VN, into the protograph;
(5) Select the protograph (i.e., base matrix) with the lowest decoding threshold among all the protographs satisfying the aforementioned constraints.

2) Design of protograph codes with VN-degrees at least 3: The conventional LDPC codes and the protograph codes with such a constraint are guaranteed to have linear minimum distance [12], [50], [96]. The design of such type of protograph codes can start from a rate-$1/2$ $(3, 6)$ regular protograph code with a structure shown in Fig. 7(a), which contains 8 VNs and 4 CNs. The decoding threshold of the code is 1.103 dB. To lower the threshold, one can increase the degree of a VN in Fig. 7(a) to 16 according to the discussion in Sect. III-A1 (adding a high-degree VN) and hence obtain a new protograph, i.e., Fig. 7(b). The protograph code corresponding to Fig. 7(b) possesses a decoding threshold of 0.959 dB and hence achieve a small gain of 0.144 dB over the regular protograph code. Aiming at further improvement, a re-permuting is performed on the edges connecting the remaining 7 VNs and the 4 CNs. After a simple computer search, an optimized protograph [50], [96] with a decoding threshold of 0.617 dB is produced, which is shown in Fig. 7(c). This protograph code not only has a satisfactory threshold but also preserves the linear-minimum-distance property. It is possible to find a protograph code with an even lower threshold by further increasing the optimization space (e.g., start the optimization from a $(3, 6)$ regular protograph code corresponding to a protograph with 12 VNs and 6 CNs).

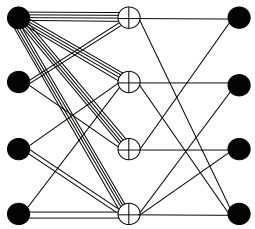

Fig. 8. The protograph of a rate-$1/2$ optimized protograph code with VN-degrees at least 2.

3) Design of protograph codes with VN-degrees at least 2: As mentioned in Sect. III-A2, the design of protograph codes is very sensitive to degree-2 VNs. On one hand, a substantial proportion of degree-2 VNs helps improving the decoding threshold. On the other hand, too many degree-2 VNs may deteriorate the linear-minimum-distance property. Consequently, the degree-2 VNs should be carefully inserted into the protograph so as to obtain the best threshold without losing the linear minimum distance.

It was proved by Abu-Surra *et al.* that a certain class of protograph codes with degree-2 VNs should retain the linear-minimum-distance property [51]. Consider a protograph code with some degree-2 VNs, we extract the sub-graph which only contains the degree-2 VNs as well as the associated CNs and edges. The protograph code can benefit from the linear minimum distance if no loop exists in the sub-graph. To ensure the linear-minimum-distance property, one can optimize the threshold performance in such a class of protograph codes.

Alternatively, based on a protograph code with VN-degrees at least 3, Divsalar *et al.* [50] have proposed a CN-splitting technique to increase the proportion of degree-2 VNs in the protograph while maintaining the linear minimum distance. Utilizing such a technique, a rate-$1/2$ protograph code that achieves a low decoding threshold (i.e., 0.502 dB) as well as a linear minimum distance has been optimized in [50][9]. The structure of this protograph code is illustrated in Fig. 8.

4) Design of protograph codes with VN-degrees at least 1: One can easily observe that the protographs corresponding to the optimized codes in Fig. 7(c) and Fig. 8 have a main drawback. They do not consider a precoding structure. A precoding structure can improve both the decoding threshold and the linear minimum distance. The first attempt to utilize a precoding structure is the construction of the AR3A code [98]. Referring to Fig. 3(a), the protograph of the rate-$1/2$ AR3A code is obtained by adding a precoding structure into the rate-1/2 RA code. Although the decoding threshold is remarkably improved by this method, the rate-$1/2$ AR3A code possesses too many degree-2 VNs, i.e., two degree-2 VNs in every five VNs. These degree-2 VNs and the associated CNs and edges form a loop of girth-4[10] and hence the AR3A code cannot

[9]The detailed optimization procedure is omitted here for simplicity.

[10]In a protograph, the girth is also defined as the length of the shortest cycle.

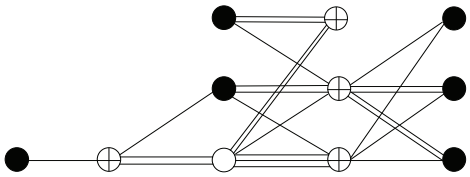

Fig. 9. The protograph of a rate-$1/2$ optimized protograph code with VN-degrees at least 1.

satisfy the condition for linear minimum distance. To address this problem, the AR4JA code is constructed by decreasing the number of degree-2 VNs in order to recover the linear-minimum-distance property. It can be seen from Fig. 3(b) that the rate-$1/2$ AR4JA code just has one degree-2 VN in every five VNs.

Yet, there is room for further improvement since the AR4JA code has not been optimized by a systematic search for a given design space. As a result, an optimized rate-$1/2$ protograph code has been constructed in [61]. To increase the search space, the authors have first initialized the optimization with a 4×7 base matrix (rather than a 3×5 base matrix), including one precoding structure (i.e., degree-1 VN), one punctured VN, and one degree-2 VN, which is expressed by

$$\mathbf{B} = \begin{pmatrix} 1 & b_{1,2} & b_{1,3} & b_{1,4} & b_{1,5} & b_{1,6} & 0 \\ 0 & b_{2,2} & b_{2,3} & b_{2,4} & b_{2,5} & b_{2,6} & 1 \\ 0 & b_{3,2} & b_{3,3} & b_{3,4} & b_{3,5} & b_{3,6} & 1 \\ 0 & b_{4,2} & b_{4,3} & b_{4,4} & b_{4,5} & b_{4,6} & 0 \end{pmatrix}, \tag{7}$$

where the first column, the second column, and the last column correspond to the degree-1 VN, the punctured highest-degree VN, and the degree-2 VN, respectively. To limit the search space, only one degree-2 VN is considered in this protograph which ensures the linear minimum distance, i.e., columns $2 \sim 6$ correspond to the VNs with degrees at least 3. The value of $b_{i,j}$ $(1 \leq i \leq 4, 2 \leq j \leq 6)$ is assumed as $0 \leq b_{i,j} \leq 3$ to keep the low complexity of the protograph code, i.e., $b_{i,j} \in \{0, 1, 2, 3\}$. Therefore, one can get the optimized base matrix after a simple search as [61]

$$\mathbf{B} = \begin{pmatrix} 1 & 2 & 1 & 0 & 0 & 0 & 0 \\ 0 & 3 & 1 & 0 & 1 & 1 & 1 \\ 0 & 1 & 2 & 1 & 2 & 2 & 1 \\ 0 & 2 & 0 & 2 & 0 & 0 & 0 \end{pmatrix}. \tag{8}$$

The protograph of this rate-$1/2$ optimized code is shown in Fig. 9. This optimized protograph code accomplishes a decoding threshold of 0.395 dB, which has a gap of 0.208 dB to the channel capacity.

In the end, we compare the BER performance of the three rate-$1/2$ optimized protograph codes introduced in this subsection with information length $K = 1024$ in an AWGN channel and show the results in Fig. 10. Referring to this figure, the optimized protograph code with VN-degrees at least 1 is the best-performing code while the optimized protograph code with VN-degrees at least 3 is the worst-performing one. Furthermore, all the three protograph codes do not show error floors at a BER of 5×10^{-7}.

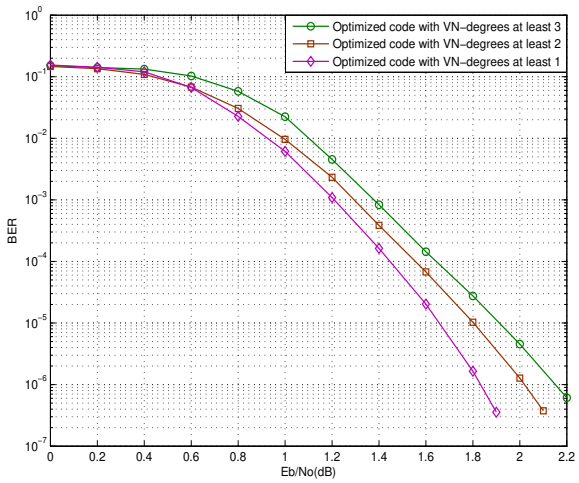

Fig. 10. BER curves of the three rate-$1/2$ optimized protograph codes with information length $K = 1024$ in an AWGN channel.

C. Design of RCP Codes

In this subsection, some methodologies for designing RCP codes are introduced. Strong RC codes are important to achieve high throughput in HARQ systems[11] [84], [127]. The RCP codes were first studied in [48], [49], in which the families of nested AR3A code and AR4JA code with a code rate $R = (n+1)/(n+2)$ $(n = 0, 1, \ldots)$ have been proposed. These two types of codes cover a wide range of code rates from $1/2$ to $1 - \zeta$ (ζ is an arbitrarily small positive value). However, they are unsuitable for HARQ applications because the information length is not kept constant for different code rates. To resolve this problem, several families of truly RCP codes have been proposed for HARQ systems [50], [59]–[62].

Actually, the RCP codes can be built by expurgation (puncturing) and extension (lengthening). Puncturing can produce a family of higher-rate RCP codes from a low-rate protograph code, while lengthening can generate a family of lower-rate RCP codes from a high-rate protograph code. Both methods maintain the same number of information bits as the code rate varies. Using the aforementioned techniques, a family of RCP codes with code rates ranging from $1/2$ to $16/17$ have been constructed in [59], but with a relatively large gap (i.e., about 0.5 dB) to the capacity. We now introduce two good designs of RCP codes by using expurgation and extension, respectively.

1) Design of RCP codes via expurgation: Based on the rate-$1/2$ optimized protograph code in Fig. 7(c), a family of higher-rate RCP codes, denoted as *RCP1 codes*, which possess low decoding threshold and linear minimum distance, have been constructed via adding additional punctured-degree-2 VNs [50]. The protograph of the RCP1 code is presented in Fig. 11.

[11] Automatic repeat request (ARQ) is an error-control mechanism for data-transmission. It requests the data-link layer of the transmitter to retransmit packets that have not been correctly received by the receiver. This technique is of great usefulness to enhance the error performance and system throughput, and therefore has been extensively exploited by a myriad of wireless communication systems and standards, such as Long Term Evolution (LTE) in 4G wireless communication systems [125]. As a promising variant of ARQ, HARQ combines the ARQ principle with FEC codes [126]. The main difference between ARQ and HARQ is that the original information can be encoded by a FEC code before transmission in the latter one.

TABLE V
DECODING THRESHOLDS $(E_b/N_0)_{\rm th}$ (dB) AND CAPACITY GAPS OF THE RCP1 CODE WITH DIFFERENT CODE RATES $R = 1/2, 5/8, 3/4$, AND $7/8$.

R	$1/2$	$5/8$	$3/4$	$7/8$
$(E_b/N_0)_{\rm th}$	0.617	1.301	1.932	3.051
Capacity	0.187	0.815	1.626	2.845
Δ	0.430	0.486	0.306	0.206

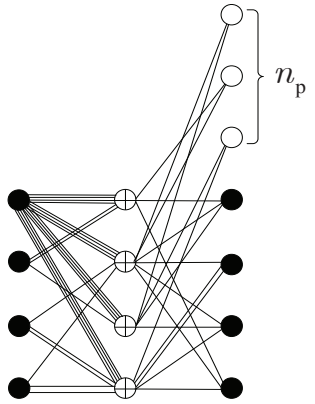

Fig. 11. The protograph of a RCP1 code.

The RCP1 code has a code rate of $R = (4 + n_{\rm p})/(N_{\rm P} - n_{\rm p})$, where $n_{\rm p} \in \{0, 1, 2, 3\}$ is the punctured length and $N_{\rm p}$ is the number of VNs in the protograph. Moreover, we show the decoding thresholds and the capacity gaps[12] of the RCP1 code with different code rates in Table V, from which we observe that the capacity gap of the code varies from 0.430 dB to 0.486 dB, 0.306 dB, and 0.206 dB, respectively, as R increases from $1/2$ to $5/8, 3/4$, and $7/8$.

2) Design of RCP codes via extension: In [61], the authors have proposed a new family of RCP codes that cover a wide code-rate range by extending the base matrix (8). To begin with, a rate-$5/6$ protograph code is designed by introducing more columns (i.e., VNs) to the existing base matrix (8), resulting in

$$\mathbf{B}' = \left(\begin{array}{c|cccccccccccc} \mathbf{B} & 0 & 1 & 1 & 0 & 0 & 1 & 0 & 1 & 2 & 0 & 0 & 0 \\ & 1 & 0 & 1 & 1 & 2 & 0 & 1 & 1 & 2 & 0 & 2 & 2 \\ & 2 & 2 & 2 & 2 & 1 & 2 & 2 & 2 & 1 & 2 & 1 & 1 \\ & 0 & 1 & 0 & 0 & 0 & 2 & 0 & 0 & 0 & 2 & 0 & 0 \end{array} \right). \quad (9)$$

The corresponding protograph contains 19 VNs and 4 CNs. The decoding threshold of this rate-$5/6$ protograph code is 2.445 dB, showing a gap of 0.083 dB to the capacity. Based on such a base matrix, a lower-rate RCP code, called as *RCP2 code*, can be extended by adding the same number of new columns (VNs) and rows (CNs) into the base matrix $\mathbf{B}'$, i.e., by adding extra parity bits into the rate-$5/6$ protograph code while keeping the information bits unchanged. Assume that the number of newly added columns/rows is $n_{\rm A}$, the code rate of the RCP2 code becomes $R = (19 + n_{\rm A} - n_{\rm A} - 4)/(19 - 1 + n_{\rm A}) = 15/(18 + n_{\rm A})$. Therefore, using the computer research, an optimized family of RCP2 codes with code rates ranging from $5/6$ to $15/(18 + n_{\rm A})$ can be generated. For example, Nguyen *et al.* [61] have constructed a family of RCP2 codes with code rates ranging from $5/6$ to $15/46$ (i.e., $n_{\rm A} = 0, 1, \ldots, 28$), all of which possess both capacity-approaching decoding thresholds (within 0.15 dB to the corresponding capacities) and linear minimum distance. Here, we do not elaborate the details of the RCP2 codes but refer the interested readers to [61].

Remark: Besides the above-mentioned results, some contributions have been made to the design of short-length RCP codes with code rates ranging from $1/3$ to $4/5$ in AWGN channels [62] and to the design of RCP codes with code rates ranging from $1/10$ to $9/10$ which perform well in both AWGN and erasure channels [60].

[12]The capacity gap is defined as the difference between the channel capacity and the decoding threshold.

D. Design of Bilayer Protograph Codes

Spatial diversity is a useful technique to improve the quality of transmission. It is well known that spatial-diversity gain can be achieved by cooperation [128]. The relay channel [129], which is the most elementary framework of cooperative communication systems, has attracted much attention in recent years. Inspired by the work of [130], bilayer protograph codes have been designed for the three-node half-duplex relay systems with decode-and-forward (DF) protocol so as to remarkably improve the error performance [101], [102]. Similar to the design of RCP codes, the capacity-approaching bilayer protograph codes can also be constructed via either expurgating (adding new rows, i.e., CNs, into a base matrix) or lengthening (adding new columns, i.e., VNs, into a base matrix). Here, we just elaborate a little further on the construction of bilayer lengthened protograph codes, while the design of bilayer expurgated protograph codes can be found in [101], [102].

In the three-node half-duplex relay channel, each transmission period involves two time slots. The transmission technique for a bilayer lengthened protograph code in such a channel is briefly described as follows. In the 1st time slot, a source (S) broadcasts a rate-$R_{\rm SR}$ protograph code $C_{\rm SR} = (C_{\rm SD}, \mathcal{V}_{\rm RD})$ to the relay (R) and destination (D), where $C_{\rm SD}$ is the sub-codeword with a code rate $R_{\rm SD}$ ($R_{\rm SD} < R_{\rm SR}$) in layer-1 and $\mathcal{V}_{\rm RD}$ is the extended information/parity bits (i.e., virtual sub-codeword) in layer-2. In the 2nd time slot, R firstly decodes $C_{\rm SR}$ and then re-encodes $\mathcal{V}_{\rm RD}$ in layer-2 with $C_{\rm RD}$ by adding some redundancy. Using the redundancy, $\mathcal{V}_{\rm RD}$ can be correctly retrieved at D. As a result, the sub-protograph in layer-2 can be removed from the whole protograph and the remaining decoding is only performed on $C_{\rm SD}$. One can refer to [101], [102], [130] for more comprehensive knowledge of bilayer coding framework.

According to such a coding technique, the overall bilayer protograph code $C_{\rm SR}$ and its corresponding sub-codeword $C_{\rm SD}$ should be carefully designed so as to achieve capacity-approaching performance in AWGN half-duplex relay channels.

Example 1: We consider a rate-$1/2$ protograph code corre-

TABLE VI
DECODING THRESHOLDS $(E_b/N_0)_{\rm th}$ (dB) AND CAPACITY GAPS OF THE OPTIMIZED BILAYER LENGTHENED PROTOGRAPH CODES [102] WITH CODE RATES $R_{\rm SR} = 2/3, 3/4, \ldots, 9/10$.

$R_{\rm SR}$	$(E_b/N_0)_{\rm th}$	Capacity	Δ
2/3	1.223	1.059	0.164
3/4	1.720	1.626	0.094
4/5	2.136	2.040	0.096
5/6	2.455	2.362	0.093
6/7	2.718	2.625	0.093
7/8	2.914	2.845	0.099
8/9	3.125	3.042	0.083
9/10	3.295	3.199	0.096

sponding to the following base matrix [102]

$$\mathbf{B} = \begin{pmatrix} 1 & 2 & 1 & 0 & 0 & 0 & 0 \\ 0 & 3 & 1 & 1 & 1 & 1 & 0 \\ 0 & 1 & 1 & 2 & 2 & 2 & 1 \\ 0 & 2 & 0 & 0 & 0 & 0 & 2 \end{pmatrix}, \tag{10}$$

where the second column corresponds to the punctured VN. This protograph code benefits from a decoding threshold of 0.439 dB and the linear-minimum-distance property. The capacity-approaching bilayer lengthened protograph code with a code rate $R_{\rm SR} = (n+1)/(n+2)$ $(n = 1, 2, \ldots)$ can be obtained by executing the computer research on an extended base matrix of $\mathbf{B}$, expressed as

$$\mathbf{B}^n_{\rm SR} = \left(\begin{array}{c|ccc} \mathbf{B}^n_{\rm SD} & b_{1,1} & b_{1,2} & b_{1,3} \\ & b_{2,1} & b_{2,2} & b_{2,3} \\ & b_{3,1} & b_{3,2} & b_{3,3} \\ & b_{4,1} & b_{4,2} & b_{4,3} \end{array} \right), \tag{11}$$

where $\mathbf{B}^n_{\rm SD}$ is the base matrix corresponding to the rate-$n/(n+1)$ sub-codeword $C_{\rm SD}$. During the optimization, $\mathbf{B}^n_{\rm SD}$ is initialized with $\mathbf{B}^1_{\rm SD} = \mathbf{B}$ for the 1st optimization, but is assumed to $\mathbf{B}^n_{\rm SD} = \mathbf{B}^{n-1}_{\rm SR}$ $(n \geq 2)$ for further optimization. For example, in the 1st optimization, we assume that $\mathbf{B}^1_{\rm SD} = \mathbf{B}$ and obtain an optimized $\mathbf{B}^1_{\rm SR}$ with a code rate $R_{\rm SR} = 2/3$; we then assume $\mathbf{B}^2_{\rm SD} = \mathbf{B}^1_{\rm SR}$ for the 2nd optimization and get $\mathbf{B}^2_{\rm SR}$ with a code rate $R_{\rm SR} = 4/5$, and so on. The optimization results of the bilayer lengthened protograph codes with code rates $R_{\rm SR} = 2/3, 3/4, \ldots, 9/10$, which possess capacity-approaching decoding thresholds, have been obtained in [102]. Their corresponding decoding thresholds and capacity gaps are presented in Table VI, from which we observe that all the optimized bilayer lengthened protograph codes have very low thresholds — within 0.083 to 0.164 dB of their corresponding capacities.

E. Design of other variants of Protograph Codes

Several meritorious variants of protograph codes, such as non-binary protograph codes, generalized protograph codes, protograph-based convolutional codes, PBRL codes, and SCPB codes have also been proposed, analyzed, and designed in [66]–[69], [54]–[57], [71]–[73], [74]–[76], and [77], [78], respectively, due to the advantages of protograph codes. All the variants can outperform the existing (binary) protograph codes under different scenarios. However, we mainly focus our attention on the binary protograph codes in this survey. The detailed design of the non-binary protograph codes, generalized protograph codes, protograph-based convolutional codes, RBRL codes, and SCPB codes is outside the scope of this paper. Therefore, we refer the interested readers to the aforementioned publications as well as the references therein for further reading.

F. Conclusions

In this section, we have elaborated the detailed design of protograph codes for AWGN channels. In Sect. III-A, we have concluded the properties of a good protograph code. Subsequently, a generalized design scheme has been proposed in order to construct good fixed-rate protograph codes in Sect. III-B. The codes not only possess capacity-approaching thresholds, but also maintain the linear-minimum-distance property. We have also outlined the design of RCP codes in Sect. III-C and the construction of bilayer protograph codes in Sect. III-D. Moreover, we have shown that bilayer protograph codes are particularly suitable for half-duplex relay systems. In Sect. III-E, we have briefly introduced some meritorious variants of protograph codes.

IV. DESIGN OF PROTOGRAPH CODES IN OTHER TYPES OF CHANNELS

Owing to the superior performance of protograph codes in AWGN channels, they have been further applied to other types of channels, i.e., ergodic fading channels, non-ergodic BF channels, PR channels, and Poisson PPM channels. In this section, we elaborate the design and analyses of protograph codes in such scenarios.

A. Design of Protograph Codes in Ergodic Fading Channels

Protograph codes can be exploited to significantly enhance the reliability of signal transmission over fading channels. [106] is the first related work that considers the protograph codes in the context of fading. Yet, the design and analysis of protograph-based BICM in [106] is only conducted in AWGN channels, and the method used is the same as that in AWGN channels without any modification. Hence, the proposed protograph-based BICM framework may not be usable for fading channels.

Later, protograph codes have been intensely investigated over different ergodic fading channels, e.g., single-input multiple-output (SIMO) fading channels and relay fading channels, in terms of convergence speed and asymptotic BER [107], [108]. In particular, the work in [108] has assumed that the transmitted signal suffers from a Nakagami fading due to the fact that fading statistics in practical wireless communications are more suitably described by a Nakagami distribution [131], [132]. For this reason, we assume that the fading gain in all the fading channels considered in this paper follows a Nakagami-m distribution without loss of generality.

Furthermore, as proved in [20], LDPC codes which perform well in AWGN channels also perform well in other memoryless channels. This is also true for protograph codes. Accordingly, the protograph codes that possess excellent performance in AWGN channels can perform well in ergodic

TABLE VII
DECODING THRESHOLDS E_b/N_0 (dB) AND CAPACITY GAPS Δ OF THE RATE-1/2 AR3A CODE, AR4JA CODE, REGULAR $(3,6)$ CODE, AND OPTIMIZED IRREGULAR LDPC CODE IN A NAKAGAMI ERGODIC FADING CHANNEL WITH FADING DEPTH $m = 1$.

Capacity	Regular		Irregular [36]		AR3A		AR4JA	
	$(E_b/N_0)_{\text{th}}$	Δ	$(E_b/N_0)_{\text{th}}$	Δ	$(E_b/N_0)_{\text{th}}$	Δ	$(E_b/N_0)_{\text{th}}$	Δ
1.834	2.978	1.144	2.095	0.261	2.163	0.329	2.321	0.487

fading channels without any further optimization. Based on this conclusion, there is no need to re-design the protograph codes for ergodic fading channels. For instance, as shown in [48], [49], the AR3A code is one of the best-performing protograph codes in the waterfall region ($\text{BER} \geq 10^{-6}$) in an AWGN channel, and hence it may also exhibit desirable error performance in an ergodic fading channel (see the forthcoming Fig. 12). As in AWGN channels, the AR3A code may have an error floor at a low BER-level (e.g., $\text{BER} \leq 3\times10^{-6}$) in an ergodic fading channel. Yet a code like AR3A code that possesses excellent error performance down to a BER of 10^{-5} can satisfy the requirement for most wireless communication applications [133]. As a consequence, most contributions related to protograph codes in ergodic fading channels restrict their effort to the analysis aspect [107], [108]. In this subsection, we assume that the channel fading gain is changing sufficiently rapidly so as to satisfy the ergodicity [18].

1) Modified PEXIT algorithm: One important assumption of the EXIT algorithm is that the channel initial LLR messages should follow a symmetric Gaussian distribution [17]. Unfortunately, it can be easily demonstrated that the symmetric Gaussian assumption cannot be maintained in the context of ergodic fading and the PEXIT algorithm in [58] is no longer useful for such channels.

However, for a fixed channel fading gain, the channel initial LLR messages do follow a symmetric Gaussian distribution. As a result, one can randomly generate Q (Q is a sufficiently large positive integer) fading gains $\alpha_{q,j}$ $(q = 1, 2, \ldots, Q, j = 1, 2, \ldots, N_{\text{P}})$, and compute Q different a-posteriori MI values for each VN corresponding to the Q fading gains, respectively. Afterwards, the mean of these a-posteriori MI values is calculated to determine the average decoding threshold for protograph codes. Using this idea, a modified PEXIT algorithm that can be adopted to analyze the protograph codes over ergodic fading channels has been proposed in [107].

Example 2: The decoding thresholds and capacity gaps of the rate-1/2 AR3A code and AR4JA code in a Nakagami ergodic fading channel with fading depth $m = 1$ are calculated and listed in Table VII. For comparison, the $(3, 6)$ regular LDPC code and the optimized irregular LDPC code with $d_{v_j,\max} = 10$ in [36] are also considered to gauge the performance. The results in the table indicate that the decoding threshold of irregular LDPC code is smallest and hence it should possess relatively better performance in the low-SNR region. However, the irregular LDPC code may be outperformed by other codes in the high-SNR region. Also, the regular LDPC code possesses the largest decoding threshold and is expected to be inferior to other codes in the low-SNR region. Between the AR3A code and the AR4JA code, the former one has a lower threshold.

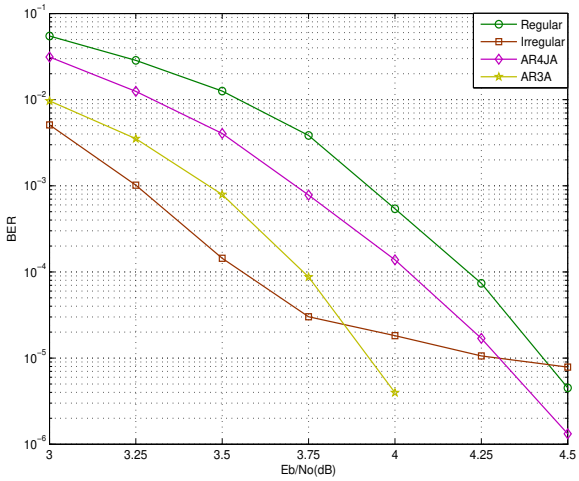

Fig. 12. BER curves of the AR3A code, AR4JA code, regular LDPC code, and irregular LDPC code in a Nakagami ergodic fading channel. The parameters used are $R = 1/2$, $K = 1024$, and $m = 1$.

Fig. 12 further depicts the BER curves of the four rate-1/2 codes with information length $K = 1024$ in a Nakagami ergodic fading channel with $m = 1$. It is observed that the irregular code has a gain of about 0.15 dB over the AR3A code at a BER of 10^{-4}, which possesses better performance than the other two codes. Yet, the BER of the irregular LDPC code has little improvement when it achieves 5×10^{-5} and thus the error floor emerges. In the same figure, the AR3A code exhibits excellent error performance for the range of E_b/N_0 under study. Moreover, no error floor exists for both AR3A code and AR4JA code at a BER of 4×10^{-6}. For a typical wireless communication channel, having no error floor at a BER of 4×10^{-6} is quite sufficient [133]. Thus, we conclude that the AR3A code stands out as a good alternative for ergodic fading channels.

2) Asymptotic error-performance: The asymptotic error-performance is also a vitally important research topic in the coding community. Based on the modified PEXIT algorithm, the authors in [108] have derived the asymptotic BER of the protograph codes in ergodic fading channels by exploiting Gaussian approximation [134]. The average BER of a protograph ensemble after t iterations is expressed by

$$P_{\text{b}}^{t+1} = \frac{1}{2N_{\text{P}}} \sum_{j=1}^{N_{\text{P}}} \text{erfc}\left(\frac{J^{-1}(\bar{I}_{app}^{t+1}(j))}{2\sqrt{2}} \right), \qquad (12)$$

where $\bar{I}_{app}^{t+1}(j) = \mathbb{E}[I_{app,q}^{t+1}(j)] = (1/Q)\sum_{q=1}^{Q} I_{app,q}^{t+1}(j)$, Q is the number of channel-fading-gain samples, $I_{app,q}^{t+1}(j)$ is the a-posteriori MI of the j-th VN after t iterations for the q-th fading gain, obtained as [107, eq.(21)]. Exploiting (12), one

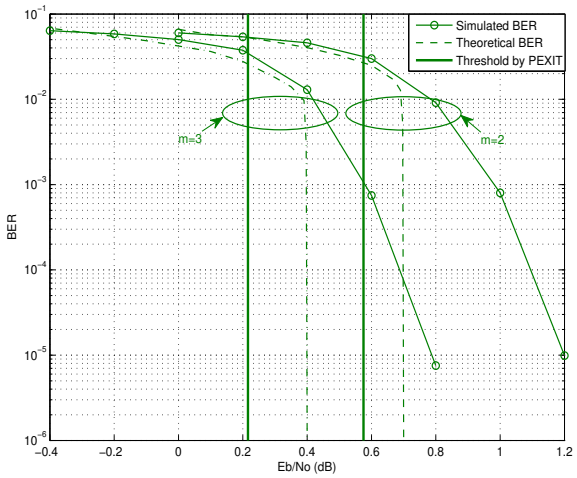

Fig. 13. BER results of the AR3A code in a Nakagami ergodic fading relay channel with EF protocol. The parameters used are $R = 4/5$, $K = 7200$, and $m = 2$ and 3. The theoretical BER is found by (12) and the decoding threshold is obtained by the PEXIT algorithm.

can evaluate the asymptotic BER for a specific protograph ensemble over ergodic fading channels. This formula has also been generalized to the half-duplex relay systems with DF and EF protocols in [108].

Remark: The maximum number of iterations in the asymptotic BER analysis (denoted as $T_{\mathrm{A,max}}$) equals the maximum number of simulated BP iterations and is much smaller than that in the modified PEXIT algorithm (denoted as $T_{\max}$). Therefore, its computational complexity is reduced by $(T_{\max} - T_{\mathrm{A,max}})/T_{\max}$ as compared with the modified PEXIT algorithm. Moreover, the BER analysis can be exploited to evaluate the error performance for any given E_b/N_0 and $T_{\mathrm{A,max}}$, while the modified PEXIT algorithm is only used to derive the decoding threshold for a sufficiently large $T_{\max}$.

Example 3: The BER results of the rate-$4/5$ AR3A codes with information length $K = 7200$ in a Nakagami ergodic fading relay channel[13] with EF protocol are plotted in Fig. 13. The fading depths m are set to 2 and 3. Referring to this figure, at a BER of 10^{-5}, the difference between the theoretical E_b/N_0 based on (12) and the decoding threshold obtained by the PEXIT algorithm is less than 0.2 dB for both fading depths. Further the simulated E_b/N_0 has another gap of around $0.4 \sim 0.5$ dB compared to the theoretical one — the reason being that the theoretical BER by (12) is derived based on the infinite-codeword-length assumption. These results agree well with those shown in [134] and [135]. In general, the theoretical expression in (12) not only can give a nice approximation for the BER of the codes with large codeword length, but also can be used to approximate the decoding threshold with a reasonable accuracy.

B. Design of Protograph Codes in Non-Ergodic BF Channels

Distinguished from ergodic fading channels, the BF channel is non-ergodic and can be considered as a type of memory channel. In a BF channel, the fading gains remain constant on each fading block and take different independent-and-identically-distributed random variables on different fading blocks. Since the BF channel is not information stable, one can only use the outage probability rather than the Shannon capacity to measure the fundamental limit for such a channel given a sufficiently large codeword length [136]. Due to the non-ergodicity, the capacity-approaching LDPC codes in AWGN and ergodic fading channels can no longer possess outstanding performance in a BF channel. Recently, Boutros *et al.* [137] has provided a solution to design full-diversity[14] LDPC codes so as to obtain superior performance in the BF channels. In detail, a family of structured LDPC codes, namely *root-LDPC codes*, which can achieve full-diversity and approach the outage limit, have been proposed based on a special type of CNs, called *rootcheck*. In [109], the protograph codes have been applied to BF channels for the first time, and a novel PEXIT algorithm has been proposed for such scenarios. Motivated by this work, several contributions related to the design of protograph codes in BF channels have been carried out [110]–[112].

1) Design of RP codes for point-to-point BF channels: In a BF channel, the received signal corresponding to the j-th coded bit can be mathematically expressed as

$$y_j = \alpha_l x_j + n_j, \tag{13}$$

where $l = 1 + \lfloor (j-1)/B \rfloor$ denotes the l-th fading block, $B = N/L$ is the block length (i.e., the number of coded bits in each fading block), L ($L \geq 2$) is the number of fading blocks, x_j is the j-th BPSK modulated bit, and n_j is the Gaussian noise that follows $n_j \sim \mathcal{N}(0, \sigma_n^2)$.

According to [138], the achievable diversity order d_c of a protograph code over BF channels is limited by $d_{\mathrm{c}} \leq 1 + \lfloor L(1-R) \rfloor$, where R is the code rate. Therefore, $R = 1/L \leq 1/2$ is the highest achievable code rate for a full-diversity protograph code (i.e., when $d_c = L$). Unless otherwise stated, we assume that $L = 2$ in our analysis below.

In [111], the authors have first introduced the concept of full-diversity RP codes with the help of rootchecks (rootcheck was first introduced in [137]) for BF channels. Then the detailed design of the rate-$1/2$ RP codes has been conducted. The generalized $M_{\mathrm{P}} \times N_{\mathrm{P}}$ base matrix of a rate-$1/2$ RP code is given as

$$\mathbf{B} = \begin{array}{c} \begin{array}{cc|cc} \mathcal{V}_{\mathrm{i}1} & \mathcal{V}_{\mathrm{p}1} & \mathcal{V}_{\mathrm{i}2} & \mathcal{V}_{\mathrm{p}2} \end{array} \\ \left(\begin{array}{cc|cc} \mathbf{I} & \mathbf{0} & \mathbf{H}_{\mathrm{i}2} & \mathbf{H}_{\mathrm{p}2} \\ \mathbf{H}_{\mathrm{i}1} & \mathbf{H}_{\mathrm{p}1} & \mathbf{I} & \mathbf{0} \end{array}\right) \begin{array}{c} \mathcal{C}_1 \\ \mathcal{C}_2 \end{array} \end{array} \tag{14}$$

where $N_{\mathrm{P}} = 2M_{\mathrm{P}} = 4M_{\mathrm{R}}$ and M_{R} is the number of rootchecks in every type of rootchecks. $\mathbf{I}$ and $\mathbf{0}$ are the identity matrix and zero matrix of dimensions $M_{\mathrm{R}} \times M_{\mathrm{R}}$, respectively. $\mathbf{H}_{il}$ and $\mathbf{H}_{\mathrm{p}l}$ ($l = 1, 2$) are the sub-matrices of dimension $M_{\mathrm{R}} \times M_{\mathrm{R}}$. As can be seen, the VNs are divided into four subsets: two subsets correspond to information bits, i.e., $\mathcal{V}_{\mathrm{i}1}$

[13]The model of relay channel used here is the same as that in [108], but the parameters of the codes used are different.

[14]Diversity order is of great importance to determine the word error rate (WER) in the high-SNR region of coded-BF channels. The diversity order achieved by a code is defined as $d_{\mathrm{c}} = -\lim_{\bar{\gamma} \to +\infty} (\ln P_{\mathrm{w}})/(\ln \bar{\gamma})$, where P_{w} is the WER of the code, $\bar{\gamma} = \mathbb{E}[\gamma_l] = \mathbb{E}[(E_s/N_0)\alpha_l^2]$ is the average received SNR of the l-th ($l = 1, 2, \ldots, L$) fading block, and α_l is the fading gain of the l-th fading block with $\mathbb{E}[\alpha_l^2] = 1$. A code is said to have full diversity if $d_{\mathrm{c}} = L$.

and $\mathcal{V}_{\mathrm{i}2}$, and the other two subsets correspond to parity bits, i.e., $\mathcal{V}_{\mathrm{p}1}$ and $\mathcal{V}_{\mathrm{p}2}$. The VNs $v_j \in \mathcal{V}_{tl}$ ($\mathcal{V}_{tl} = \mathcal{V}_{\mathrm{i}l} \bigcup \mathcal{V}_{\mathrm{p}l}$) are transmitted on α_l. We also define two new subsets corresponding to all the information bits and parity bits as $\mathcal{V}_{\mathrm{i}} = \mathcal{V}_{\mathrm{i}1} \bigcup \mathcal{V}_{\mathrm{i}2}$ and $\mathcal{V}_{\mathrm{p}} = \mathcal{V}_{\mathrm{p}1} \bigcup \mathcal{V}_{\mathrm{p}2}$, respectively. Similarly, the CNs are split into two subsets: $\mathcal{C}_1$ and $\mathcal{C}_2$, where $\mathcal{C}_l$ denotes the subset containing type-l rootchecks. In the RP code, the weight per-row of the combined sub-matrix $\mathbf{B}_{tl} = [\mathbf{H}_{il}\ \mathbf{H}_{\mathrm{p}l}]$ should be larger than or equal to 2. Using such a coding scheme, the information bits rather than the parity bits are protected to achieve full-diversity, which is considered as an unequal error protection (UEP).

Aiming at predicting the convergence performance and error performance of RP codes, a modified PEXIT algorithm has been proposed and an asymptotic error-performance expressions has been derived in [111]. In order to elaborate a little further on the optimization of RP codes, we now introduce two new terms.

Definition 1. The *SNR outage boundary* of a RP code is defined as $\gamma_{2,\mathrm{th}} = F_{\mathrm{S}}(\gamma_{1,\mathrm{th}}, \mathbf{B})$, where $F_{\mathrm{S}}(\cdot)$ represents the SNR-threshold processor of the iterative decoder to ensure $I_{app}(j) = 1$ for all $v_j \in \mathcal{V}_{\mathrm{i}}$.

Likewise, the *fading outage boundary* of a RP code is defined as $\alpha_{2,\mathrm{th}} = F_{\mathrm{F}}(E_b/N_0, \alpha_{1,\mathrm{th}}, \mathbf{B})$ for a given E_b/N_0, where $F_{\mathrm{F}}(\cdot)$ represents the fading-threshold processor of the iterative decoder.

Definition 2. The *ergodic SNR/fading threshold* $\gamma_{\mathrm{th}}/\alpha_{\mathrm{th}}$ is defined by the intersection of the SNR/fading outage-boundary and the ergodic line, where the ergodic line is described as the curve $\gamma_1 = \gamma_2/\alpha_1 = \alpha_2$.

The outage boundary and the ergodic threshold of a protograph code can be derived by using the PEXIT algorithms in the BF channel [111] and the AWGN channel [58], respectively.

Actually, there are two properties for a good RP code: i) a lower ergodic threshold, which is only determined by the decoding threshold in AWGN channels, and ii) an outage boundary that approaches the outage bound. According to these two properties, a simple design scheme has been proposed to design the outage-limit-approaching RP codes in [111], which can be summarized as follows.

(1) Add a certain proportion of degree-2 VNs and a precoding structure, i.e., a degree-1 VN, into the RP code.
(2) Select the base matrix with the lowest outage region among the matrices that satisfy the aforementioned constraint.

Note also that

- The degree-2 VNs and the VNs in the precoding structure should be affected by the same fading gain, i.e., α_1 or α_2, so as to improve the ergodic threshold.
- Step 1 is used to satisfy the first property of a good RP code while Step 2 is employed to ensure the second one.

Utilizing such a design scheme, outage-limit-approaching RP codes can be constructed.

Example 4: Assuming a rate-$1/2$ RP code corresponding to a 4×8 base matrix, an optimized code, called *improved RP2 (IRP2) code*, has been constructed in [111], whose structure is shown in Fig. 14. In the figure, the VNs affected by α_1 and α_2 are respectively denoted as black and red circles. One can easily observe that the IRP2 code preserves the linear-minimum-distance property. The SNR outage boundaries and the fading outage boundaries of the rate-$1/2$ IRP2 code, the well-known Hamming-doped (HD) protograph code [56], AR4JA code, and $(3, 6)$ regular protograph code in a Nakagami BF channel with $L = 2$ and $E_b/N_0 = 9$ dB are plotted in Fig. 15. Also, the WER results of the four protograph codes in a Nakagami BF channel with $m = 2$ are presented in Fig. 16. Referring

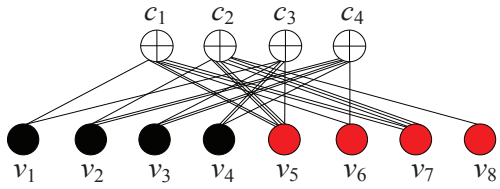

Fig. 14. The protograph of an IRP2 code.

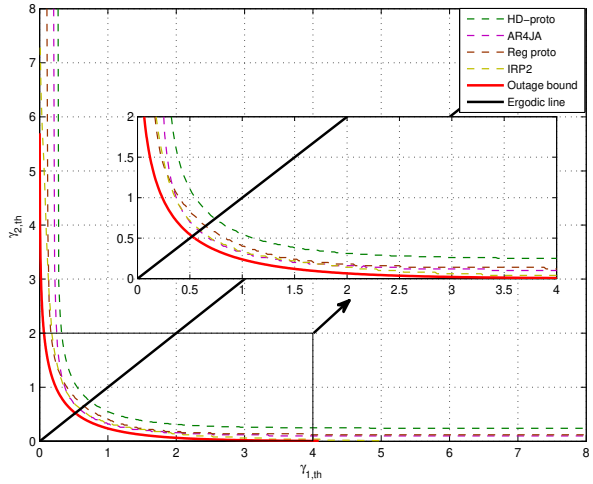

(a)

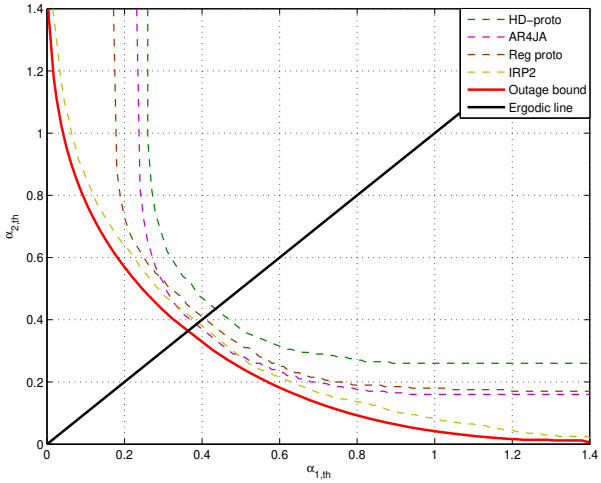

(b)

Fig. 15. The (a) SNR outage-boundaries and (b) fading outage-boundaries of the HD-protograph code, AR4JA code, regular protograph code, and IRP2 code in a Nakagami BF channel. The parameters used are $R = 1/2$, $L = 2$, and $E_b/N_0 = 9$ dB.

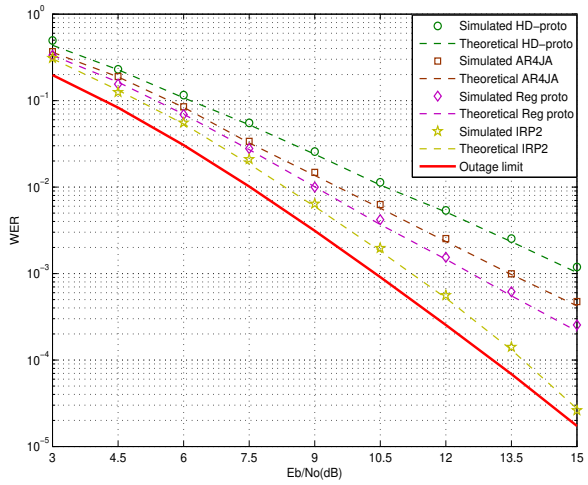

Fig. 16. WER results of the HD-protograph code, AR4JA code, regular protograph code, and IRP2 code in a Nakagami BF channel. The parameters used are $R = 1/2$, $K = 1024$, $m = 2$, and $L = 2$.

to Fig. 15, the HD-protograph code and AR4JA code, which have shown to possess outstanding performance in AWGN channels, have their outage boundaries furthest away from the outage bounds. Furthermore, these boundaries do not converge to zero as γ_l/α_l approaches infinity, implying that these codes produce finite outage probabilities even when γ_l/α_l is very large. These codes are therefore the worst-performing ones among the four protograph codes over BF channels in terms of outage performance. The outage boundaries of the regular protograph code also do not converge to zero as γ_l/α_l approaches infinity but are relatively close to the bounds as compared with the previous two. For the IRP2 code, not only are its outage boundaries closest to the bounds, but also approach the bounds and converge to zero very quickly as γ_l/α_l increases. Thus, the IRP2 code is the best-performing one among the four protograph codes. The WER results in Fig. 16 further validate the above conclusions. In particular, the results show that the WER of the IRP2 code is very close to the limit.

2) Design of protograph codes for relay BF channels: As introduced in Sect. III-D, the relay channel stands out as a typical framework for cooperative communications. Exploiting the relay, spatial diversity can be achieved so as to mitigate the effect of fading in wireless communication systems. Parallel the information-theoretic advancements, the relaying protocols such as DF and amplify-and-forward have been developed [128], [139]. As a variant of DF, coded cooperation (CC) is a better and more spectral-efficient protocol [140]. Recently, the protograph codes have been designed for CC protocol in relay BF channels, i.e., quasi-static fading (QSF) relay channels, where the fading gain of a given link is constant for each transmission period, but varies for different transmission periods [110], [112].

Similar to the BF channel, the code rate of a full-diversity code in QSF relay channels should be satisfying $R_c \leq 1/d_{\rm c} = 1/N_{\rm u}$, where $N_{\rm u}$ represents the total number of source and relays. For a three-node half-duplex relay channel, we have $N_{\rm u} = 2$ and $R_c \leq 1/2$.

Employing the UEP property (i.e., unequal diversity), a novel construction method for high-rate unequal-diversity protograph codes has been introduced in QSF relay channels with CC protocol [110]. The unequal-diversity protograph code, which is considered as a type of bilayer protograph codes [101], [102], can be constructed by concatenating two IRA/RA codes. As observed, the authors in [112] have designed several rate-$7/10$ unequal-diversity protograph codes.

Example 5: The base matrices of two optimized constituent IRA codes with code rates $R_{\rm S} = 7/8$ and $R_{\rm R} = 1/2$, and the corresponding overall unequal-diversity protograph code with a code rate $R_c = 7/10$ in [110] are, respectively, given by

$$\mathbf{B}_{\rm S} = \begin{pmatrix} 16 & 6 & 3 & 3 & 3 & 3 & 3 & 2 \end{pmatrix}, \quad \mathbf{B}_{\rm R} = \begin{pmatrix} 2 & 1 & 1 \\ 1 & 1 & 1 \end{pmatrix},$$
$$\mathbf{B} = \begin{pmatrix} 16 & 6 & 3 & 3 & 3 & 3 & 3 & 2 & 0 & 0 \\ 2 & 0 & 0 & 0 & 0 & 0 & 0 & 0 & 1 & 1 \\ 1 & 0 & 0 & 0 & 0 & 0 & 0 & 0 & 1 & 1 \end{pmatrix}, \tag{15}$$

where the VNs corresponding to the first column of $\mathbf{B}$ belong to the high-priority fragment which achieves diversity-2[15]. The remaining VNs in $\mathbf{B}$ belong to the low-priority fragment. Moreover, the VNs corresponding to the first column of $\mathbf{B}_{\rm R}$ are punctured.

Although the high-priority fragment of the unequal-diversity protograph code achieves diversity-2 (diversity-2 is the full-diversity order in a QSF relay channel), the coding efficiency is relatively low (i.e., only one of the ten VNs in the protograph belongs to high-priority fragment, thus the coding efficiency is $1/10$). More importantly, the overall unequal-diversity protograph code cannot possess full-diversity in QSF relay channels because the code rate $R_c > 1/2$. To address this problem, the authors in [112] have proposed a family of full-diversity RCRP codes for QSF relay channels based on the previously introduced RP codes in Sect. IV-B1.

A full-diversity rate-R_c ($R_c \leq 1/2$) RCRP code can be constructed by adding redundancy into a given rate-$1/2$ RP code with base matrix $\mathbf{B}_{\rm RP}$. More specifically, the base matrix $\mathbf{B}$ of the rate-R_c RCRP code is produced by inserting the same number of new columns (i.e., VNs) and new rows (i.e, CNs) into $\mathbf{B}_{\rm RP}$. In a QSF relay channel, each transmission period is divided into two time slots. To implement the CC protocol, the information bits $v_j \in \mathcal{V}_{\rm i}$ are first encoded by a rate-$1/2$ RP code $C_{\rm RP} = (\mathcal{V}_{\rm t1}, \mathcal{V}_{\rm t2})$ with $\mathbf{B}_{\rm RP}$, where $v_j \in \mathcal{V}_{tl} \subseteq C_{\rm RP}$ is prepared for the transmission in the l-th time slot. Aiming at providing reliable transmissions, these VNs are re-encoded by two rate-R_1 protograph codes, i.e., $C_1 = (\mathcal{V}_{\rm t1}, \mathcal{V}_{\rm p1'})$ and $C_2 = (\mathcal{V}_{\rm t2}, \mathcal{V}_{\rm p2'})$, respectively. The two sets of newly added parity bits, i.e., $\mathcal{V}_{\rm p1'}$ and $\mathcal{V}_{\rm p2'}$, are determined only by their corresponding base matrices, i.e., $\mathbf{B}_{\rm 1S}$ and $\mathbf{B}_{\rm 1R}$, of C_1 and C_2, respectively. These two resultant sub-codewords (called frames) constitute the whole rate-R_c ($R_c = R_1/2$) RCRP code, denoted as $C = (C_1, C_2)$. As a result, S broadcasts C_1 to R and D in the 1st time slot, while R or S transmits C_2 to D in the 2nd time slot depending on the result of the first-frame (i.e., S $\rightarrow$ R) transmission. Finally, D will

[15]The high-priority fragment is defined as the VNs that are connected to the two IRA/RA protographs.

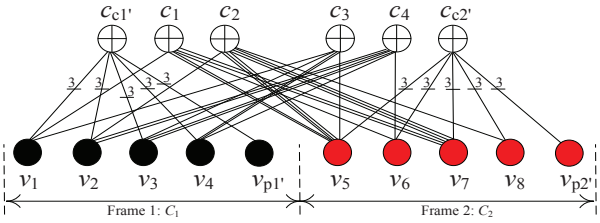

Fig. 17. The protograph of an irregular RCRP code.

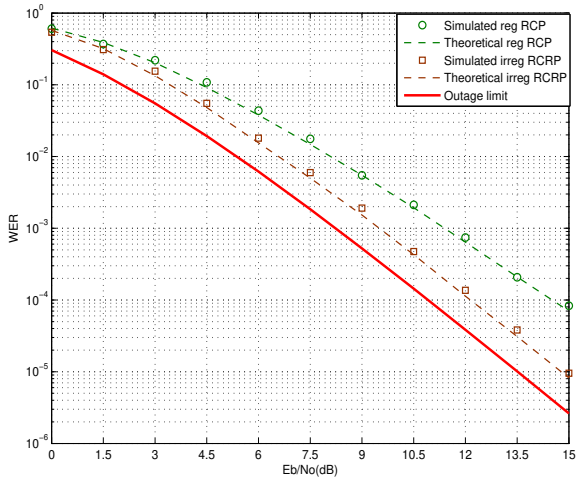

Fig. 18. WER results of the regular RCP code and irregular RCRP code in a Nakagami QSF relay channel. The parameters used are $R_c = 2/5, K = 1024, m = 2$, and $d_{\rm SR} : d_{\rm RD} : d_{\rm SD} = 0.3 : 0.7 : 1$.

use the base matrix $\mathbf{B}$ to decode the overall codeword C. One can adopt the same protograph ensemble to implement both C_1 and C_2 such that $\mathbf{B}_{1\rm S} = \mathbf{B}_{1\rm R} = \mathbf{B}_1$. Similar to RP codes, the information bits $v_j \in \mathcal{V}_{\rm i}$ and the parity bits $v_j \in \mathcal{V}_{\rm p}$ $(\mathcal{V}_{\rm p} = \mathcal{V}_{\rm p1} \bigcup \mathcal{V}_{\rm p1'} \bigcup \mathcal{V}_{\rm p2} \bigcup \mathcal{V}_{\rm p2'})$ are clearly distinguished in a RCRP code, and only the information bits are protected to have full-diversity. For simplicity, a RCRP code is referred to as a protograph code with $\mathbf{B} = (\mathbf{B}_1, \mathbf{B}_{\rm RP})$. The cooperative level of CC is $\eta = N_2/N = 1/2$, where N_2 is the codeword length of C_2. To summarize, given a rate-$1/2$ RP code, a RCRP code with a code rate R_c ranging from 0 to $1/2$ can be generated by varying the code rate R_1 of C_1.

Example 6: Consider two rate-$4/5$ codes C_1 and C_2, which belong to the same regular column-weight-3 protograph ensemble. A rate-$2/5$ irregular RCRP code can be constructed based on the rate-$1/2$ IRP2 code in Fig. 14. The protograph of such an irregular RCRP code is shown in Fig. 17. Referring to this figure, the overall protograph consists of 10 VNs and 6 CNs. Moreover, this protograph can be divided into three sub-protographs as follows: The sub-protograph of C_1 (C_2), i.e., frame 1 (frame 2), includes $v_1, v_2, v_3, v_4, v_{\rm p1'}, c_{\rm c1'}$ $(v_5, v_6, v_7, v_8, v_{\rm p2'}, c_{\rm c2'})$ and the associated edges, while the sub-protograph of $C_{\rm IRP2}$ contains $v_1, v_2, \ldots, v_8, c_1, c_2, \ldots, c_4$ and the associated edges.

Fig. 18 plots the WER results of the rate-$2/5$ irregular RCRP code and regular RCP code in a Nakagami QSF relay channel with $m = 2$. The distance ratio among the three terminals, i.e., S, R, and D, is set to $d_{\rm SR} : d_{\rm RD} : d_{\rm SD} = 0.3 : 0.7 : 1$. We observe that the proposed irregular RCRP code remarkably outperforms the regular RCP code. Furthermore, the irregular RCRP code has a gap within 1.5 dB to the outage limit for the range of E_b/N_0 under study and shows excellent error performance.

C. Design of Protograph Codes in PR Channels

As another classical type of memory channel, the PR channel [38], [39] is also well-known since it is adopted as a model for magnetic recording systems. The transfer function of such a channel is formulated as $H(D) = (1-D)(1+D)^{\kappa} = \sum_{i=0}^{\kappa+1} h_i D^i$, where κ is a non-negative integer. Thus, the channel model can be described as

$$y_j = \sum_{i=0}^{\kappa+1} h_i x_{j-i} + n_j, \tag{16}$$

where x_{j-i} is the BPSK modulated input signal, $n_j \sim \mathcal{N}(0, \sigma_n^2)$ is the Gaussian noise. FEC codes can be used to boost the error performance of the such systems. Of particular interest are the codes, e.g., protograph codes, which possess excellent error performance for high code rate [38], [48]–[52]. It is because high-rate transmission is a fundamental requirement of communications in data storage systems. Due to the inter-symbol interference (ISI), conventional protograph codes, which perform well in AWGN channels, do not perform well in PR channels. For this reason, it is necessary to redesign the protograph codes prior to applying them to such channels.

1) Design of punctured protograph codes: As illustrated in [47]–[52], the use of punctured VNs can yield significant improvement in decoding threshold of protograph codes. Therefore, the punctured protograph codes, e.g., the AR3A code and AR4JA code, have been studied in PR channels firstly. However, both codes do not show satisfactory performance in such scenarios [83], [88], [113]. To make a more insightful analysis, a new finite-length EXIT algorithm has been proposed so as to determine the convergence performance of protograph codes in PR channels [88]. Different from the conventional (infinite-length) EXIT chart [18], a finite-length EXIT chart consists of two EXIT bands. Each EXIT band composes of an expected EXIT curve, an upper-bound curve and a lower-bound curve. The EXIT band, bounded by the upper-bound curve and the lower-bound curve, is constructed to ensure that all the individual finite-length EXIT curves lie within the band with a high probability. One can conclude that the iterative decoder converges successfully with a high probability if the two EXIT bands only touch each other at the value of unity. Moreover, the region between the two expected EXIT curves is defined as the *decoding tunnel*. For a given E_b/N_0, a protograph code having a larger decoding tunnel should achieve a relatively better convergence performance.

In AWGN channels, punctured VNs with the highest degree (as in the AR3A code) can be recovered more easily than the counterparts with a lower degree. Yet, based on the EXIT analytical results of the AR3A code and AR4JA code, the authors in [83], [88] have found that this conclusion may not hold in the context of ISI. They have further conjectured that the VNs with the lowest degree may converge faster

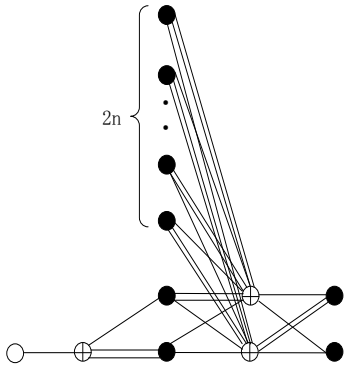

Fig. 19. The protograph of an IARA2 code.

than those with relatively higher degree. As a validation of this conjecture, four different protograph codes have been constructed using the same base matrix of the rate-$4/5$ AR3A code (see Fig. 3(a)), and are distinguished by puncturing different types of VNs, i.e., degree-1 VNs, degree-2 VNs, degree-3 VNs, and degree-5 VNs, respectively. The EXIT-chart analysis has indicated that the protograph code with punctured-degree-1 VNs obtains the largest decoding tunnel and hence should provide the best convergence performance in PR channels.

According to such a conjecture, a new approach described below has been proposed to design protograph codes in PR channels [88].

(1) Puncture the VNs with the smallest degree instead of the largest degree in the protograph code.
(2) If there are too many degree-2 VNs in the protograph code, appropriately reduce the proportion of them by adding an extra connection to some of the degree-2 VNs.

Remark: Step 1 not only can be used for designing punctured protograph code, but also can be adopted for optimizing other punctured codes in PR channels, such as the punctured turbo codes [141].

Exploiting the aforementioned design scheme, excellent protograph codes can be constructed for PR channels.

Example 7: Based on the structure of AR3A code, an improved ARA code, namely *improved ARA2 (IARA2) code* [88], has been derived via the design approach without increasing the complexity. The protograph of the IARA2 code with a code rate of $R = (n+1)/(n+2)$ $(n = 0, 1, 2, \ldots)$ is depicted in Fig. 19. As seen from this figure, the IARA2 code possesses the linear-minimum-distance property.

Assuming that a turbo decoder, which includes a Bahl-Cocke-Jelinek-Raviv (BCJR) detector (inner detector) [142] and a BP decoder (outer decoder), is used at the receiver terminal so as to alleviate the effect of ISI. The maximum numbers of turbo iterations and BP iterations (i.e, $T_{\mathrm{t,max}}$ and $T_{\mathrm{BP,max}}$) are set to 6 and 15, respectively. We compare the EXIT bands of the rate-$4/5$ IARA2 code, AR3A code, AR4JA code, and the regular column-weight-3 LDPC code [143] in a PR4 channel (i.e., $H(D) = 1 - D^2$) at $E_b/N_0 = 4.2$ dB in Fig. 20. In this figure, $I_{\mathrm{A,IO}}/I_{\mathrm{E,IO}}$ and $I_{\mathrm{A,OI}}/I_{\mathrm{E,OI}}$ denote the *a-priori/extrinsic* MIs passing from the inner detector to the outer decoder and passing from the outer decoder to

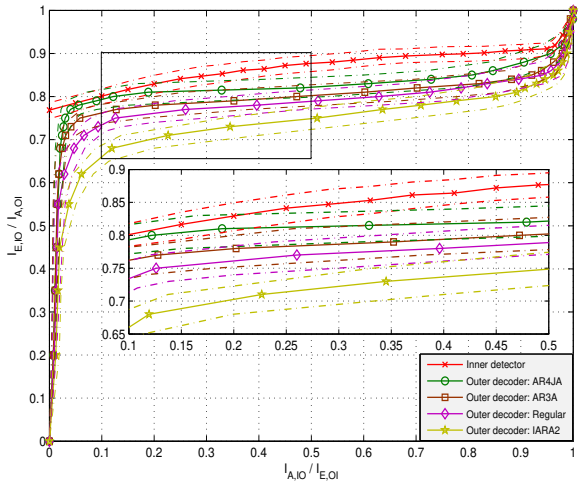

Fig. 20. EXIT bands of the IARA2 code, AR3A code, AR4JA code, and the regular column-weight-3 LDPC code in a PR4 channel. The expected EXIT curves are denoted by the solid lines, the upper-bound curves and lower-bound curves are denoted by the dotted lines. The parameters used are $R = 4/5$, $K = 4096$, $T_{\mathrm{BP,max}} = 15$, and $E_b/N_0 = 4.2$ dB.

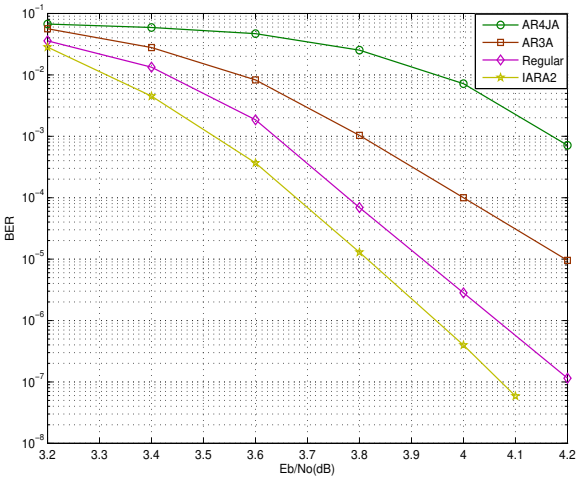

Fig. 21. Simulated BER curves of the IARA2 code, AR3A code, AR4JA code, and the regular column-weight-3 LDPC code in a PR4 channel. The parameters used are $R = 4/5$, $K = 4096$, $T_{\mathrm{t,max}} = 6$, and $T_{\mathrm{BP,max}} = 15$.

the inner detector, respectively. It reveals that the AR4JA code and AR3A code are the two worst-performing codes in this channel because of the narrowest decoding tunnels. In particular, the MI of AR4JA code cannot converge to unity at $E_b/N_0 = 4.2$ dB since the EXIT band of the inner detector partially overlaps with that of the outer decoder corresponding to the AR4JA code. Furthermore, the IARA2 code converges faster as compared to the regular column-weight-3 LDPC code, which is one of the best-performing LDPC codes in PR channels.

As a further insight, Fig. 21 plots the BER curves of these four codes in a PR4 channel. The results verify the convergence analyses and demonstrate that the IARA2 code possess excellent error performance in a PR4 channel. Simulations have also been performed in other types of PR channels, e.g., the dicode channel $(H(D) = 1 - D)$, and similar results have been obtained.

2) Design of unpunctured protograph codes: Following the works in [83], [88], [113], some research has been devoted to characterizing the performance of unpunctured protograph codes in PR channels by modifying the infinite-length EXIT algorithm, and to designing the unpunctured protograph codes that have good threshold performance [114], [115]. In [114], the authors have firstly generalized the infinite-length EXIT algorithm [58] to PR channels and have used it to calculate the decoding threshold of protograph codes. With the help of the decoding threshold metric, optimization can be performed based on a given protograph ensemble.

Example 8: Aiming at minimizing the decoding threshold, one can initialize a rate-$1/2$ protograph code without any punctured VN, which corresponds to a 4×8 base matrix with four given columns (i.e., two degree-1 VNs, one degree-2 VN, and one degree-3 VN) and four unknown columns. Subsequently, an optimized base matrix is obtained by exploiting the computer-research method described in Sect. III-B, resulting in [114]

$$\mathbf{B} = \begin{pmatrix} 2 & 2 & 0 & 0 & 0 & 0 & 0 & 1 \\ 2 & 2 & 1 & 0 & 0 & 0 & 1 & 0 \\ 2 & 2 & 2 & 1 & 1 & 1 & 0 & 0 \\ 2 & 2 & 2 & 2 & 2 & 1 & 0 & 0 \end{pmatrix}, \tag{17}$$

where the first four columns correspond to the optimized columns and the last four columns correspond to the four given columns. It is easily observed that this protograph possesses linear minimum distance. Moreover, the decoding threshold of the protograph in a dicode channel is 1.217 dB, showing a gap of 0.394 dB to the independent-and-uniformly-distributed capacity [144]. However, the code rate $1/2$ is far from that required in data storage systems. To resolve this problem, high-rate unpunctured protograph codes, e.g., $R = 4/5, 5/6, \ldots, 9/10$, have been proposed for PR channels to achieve capacity-approaching threshold [115]. Besides, a family of lower-rate RCP codes (i.e., $R = 27/(30 + n_{\mathrm{A}}),\ n_{\mathrm{A}} = 1, 2, \ldots, 11$) have been produced for PR channels based on the proposed rate-$9/10$ protograph code in the same paper.

Inspired by the above-mentioned publications, non-binary protograph codes have already been investigated over PR channels in [116], where the infinite-length EXIT algorithm has also been extended to the non-binary domain in order to measure the convergence performance (i.e., decoding threshold) of non-binary protograph codes. Nonetheless, the authors in [116] have restricted their attention to the analysis aspect and have not provided any design results.

D. Design of Protograph Codes in Poisson PPM Channels

Power efficiency is a one of the most important parameters for deep-space communications [34], [47]. Since 2003, protograph codes have been insightfully studied in perfect deep-space channels, i.e., AWGN channels. Nevertheless, the beam spreading will lead to huge power loss that makes communications in deep-space channels extremely difficult [145]. Therefore, it makes sense to combine channel coding with power-efficient techniques, e.g., PPM, in deep-space communication systems [146]. Inspired by this idea, the protograph-coded BICM-ID has been studied and optimized in Poisson PPM channels, which are used to model a direct-detection deep-space optical communications link [145], based on an extended PEXIT algorithm [103]. Although the Poisson PPM channel is a type of memoryless channel, the receiver terminal for the protograph-based BICM-ID system consists of a PPM demodulator and an LDPC decoder, which forms a turbo-like decoder (similar to the turbo decoder in Sect. IV-C). In this case, the decoding process depends on both the type of modulation and the type of channel, and the corresponding design becomes quite different from that in a memoryless channel without BICM-ID. Accordingly, the protograph codes having good performance in a particular memoryless channel, e.g., AWGN channel or ergodic fading channel, may not be applicable for the BICM-ID systems in Poisson PPM channels directly because they do not maintain their original advantages in such scenarios. In [103], the authors have first investigated the performance of several rate-$1/2$ conventional protograph-coded BICM-ID schemes in Poisson PPM channels using an extended PEXIT algorithm and have discovered that they are not able to obtain desirable decoding threshold. Then, aiming at lowering the decoding threshold of BICM-ID, the rate-$1/2$ protograph code that corresponds to a 2×4 base matrix has been optimized utilizing the computer-search method based on certain constraints.

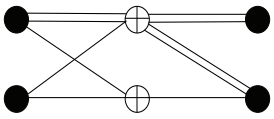

Fig. 22. The protograph of a rate-$1/2$ optimized code in a Poisson PPM channel.

Example 9: We consider a protograph with 4 VNs and 2 CNs and a 64-ary PPM modulator. Assuming that the total number of edges in the protograph is set to $10 \leq |\mathcal{E}| \leq 15$, and the number of each type of edges is less than or equal to 3, the resultant protograph of the optimized code [103] is shown in Fig. 22. In a Poisson PPM channel, the newly designed protograph-coded BICM-ID possesses a lower threshold and a better error performance as compared to i) the conventional protograph counterparts in [50], [147]; and ii) the protograph counterpart in [146] which has been developed particularly for the Poisson PPM channel and is only 0.6 dB away from capacity. *Note that* the newly designed protograph-coded BICM-ID has not considered punctured VNs and has not retained the linear-minimum-distance property.

E. Conclusions

In this section, we have turned our attention to the current research status of protograph codes under other channel conditions. Firstly, the related works on protograph codes in ergodic fading channels have been summarized in Sect. IV-A. For this case, we have found that most effort has been made in the analysis aspect because the protograph codes that perform well in AWGN channels also possess excellent performance in such scenarios. In Sects. IV-B and IV-C, we have reviewed the corresponding designs of protograph codes

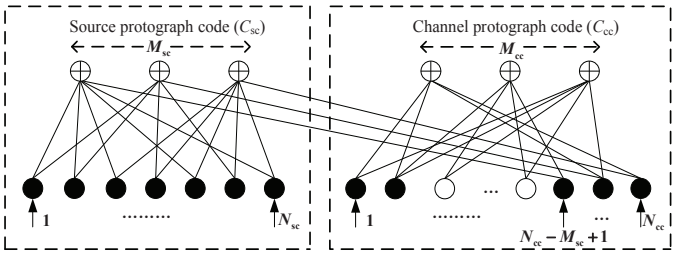

Fig. 23. The protograph of a double protograph code for JSCC.

in non-ergodic BF channels and PR channels, respectively. In particular, both point-to-point and relay frameworks have been considered in non-ergodic BF channels. Finally, the joint design of protograph codes and BICM-ID in Poisson PPM channels has been presented in Sect. IV-D.

V. Protograph-based JSCC and JCPNC

To our knowledge, the applications of protograph codes are not limited to channel coding. Protograph codes can also be used in other related areas such as JSCC and JCPNC. In this section, we provide a brief overview of the contributions that have been made in the aforementioned two areas.

A. Protograph-based JSCC

Unlike the separate design and decoding of the source-and-channel coding [148], the joint design of source-and-channel coding (i.e., JSCC) has held more attention in the past five years [149], [150]. The main idea of JSCC is that the (uncompressed or partially compressed) source is considered as redundancy and hence can be exploited by the channel decoder to improve the error performance. Motivated by the above-mentioned idea, the double LDPC code, which consists of two concatenated LDPC codes, has been proposed and optimized for JSCC [149]. The protograph codes have also been applied to JSCC [117]–[120]. Further, the construction of double protograph codes has been first elaborated in [117]. In the same work, the authors have also proposed an improved base matrix for source protograph code to enhance the error performance of protograph-based JSCC.

The overall protograph corresponding to a double protograph code is shown in Fig. 23. Referring to this figure, the information sequence $\mathbf{u}_{\rm s}$ is first compressed by an unpunctured protograph code $C_{\rm sc}$ with a $M_{\rm sc} \times N_{\rm sc}$ base matrix $\mathbf{B}_{\rm sc}$, resulting in a compressed source sequence $\mathbf{u}_{\rm sc'} = \mathbf{H}_{\rm sc}\mathbf{u}_{\rm s}$, where $\mathbf{H}_{\rm sc}$ is the parity-check matrix corresponding to the derived graph of the code $C_{\rm sc}$. Thus, the code rate of source coding is $R_{\rm sc} = M_{\rm sc}/N_{\rm sc}$. Afterwards, another punctured/unpunctured protograph code $C_{\rm cc}$ with a $M_{\rm cc} \times N_{\rm cc}$ base matrix $\mathbf{B}_{\rm cc}$ is used to re-encode $\mathbf{u}_{\rm sc'}$, and hence $C_{\rm cc}$ will be transmitted over the channel. The code rate of channel coding is $R_{\rm cc} = (N_{\rm cc} - M_{\rm cc})/(N_{\rm cc} - n_{\rm p})$, where $n_{\rm p}$ is the punctured length. *Note that* each CN in $C_{\rm sc}$ is connected to one of the last $M_{\rm cc}$ VNs in $C_{\rm cc}$ via a single edge. Using such an encoding structure, joint decoding can be performed on the corresponding derived graph of the overall double protograph code [117], [149].

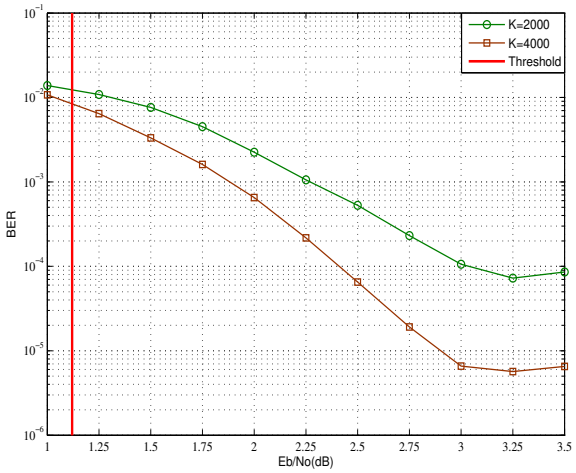

Fig. 24. Simulated BER curves and decoding thresholds of the double protograph code with different information lengths in a Nakagami ergodic fading channel. The source code and channel code are used by the rate-$1/4$ R4JA code and rate-$1/2$ AR3A code, respectively. The parameters used are $K = 2000, 4000, m = 1$, and $p_{\rm c} = 0.02$.

In certain practical applications, e.g., image transmission, some particular parts of the source information are considered as more important compared with other parts. Accordingly, it is necessary to employ different coding strategies to deal with different parts of such a source so as to protect the source information more efficiently. Recently, a novel UEP scheme has been proposed for the JSCC with double protograph code [119]. In [119], the authors have divided the source information into two different parts. Furthermore, these two parts are given two different priority levels based on their corresponding entropies. Then, they are encoded by one protograph code and one double protograph code, respectively[16].

Although the double protograph codes have been widely used for JSCC and have shown desirable performance via simulations, their analytical performance has not been adequately studied in [117]–[119]. In [120], a joint PEXIT algorithm has been proposed for evaluating the decoding threshold of double protograph codes. Moreover, the results have been extended to multi-receive-antenna-based systems over ergodic fading channels in the same paper.

Example 10: We assume that i) the rate-$1/4$ repeat-by-4-jagged-accumulate (R4JA) code [50] and rate-$1/2$ AR3A code are used as the source code and channel code, respectively, to form the double protograph code, and ii) the joint source-and-channel-decoder [117], [149] is used at the receiver terminal to estimate the original information. Fig. 24 plots the BER curves and decoding thresholds of the double protograph code with different information lengths in a Nakagami ergodic fading channel with $m = 1$. The information lengths are set to $K = 2000$ and 4000, and the crossover probability of the equivalent binary symmetric channel for the source decoder is set to $p_{\rm c} = 0.02$. As observed, the slope of the BER of the

[16]The high-priority part is not compressed by the source code and is directly encoded by the channel code, i.e., a protograph code, while the low-priority part is encoded by a double protograph code.

double protograph code is increased as K becomes larger in the low-SNR region. However, the error floor emerges for both two cases in the high-SNR region (i.e., $E_b/N_0 \geq 3.0$ dB). This error floor may vanish as K approaches infinite. Additionally, at a BER of 2×10^{-5}, the double protograph code with $K = 4000$ has a gap of about 1.6 dB to the decoding threshold.

B. Protograph-based JCPNC

Another attractive application of protograph code is in JCPNC. Physical-layer network coding (PNC) has been proposed in [151] to remarkably increase the throughput of the straightforward network coding [152]. To enhance the transmission reliability in networks based on PNC, the JCPNC frameworks implemented by RA codes and LDPC codes have been carefully designed over different types of channels [153]–[155]. Here, we present the currently achieved results of protograph-based JCPNC schemes in AWGN and fading channels [121]–[123]. Further, we propose a joint finite-length EXIT algorithm for analyzing such a JCPNC in AWGN channels.

1) Protograph-based JCPNC in AWGN channels: The protograph codes have been firstly introduced to JCPNC in [121]. In that work, the authors have proposed a serial joint channel-and-physical-layer-network decoding (JCPND) algorithm to improve the performance of standard JCPND algorithm [154]. The superiority of the newly proposed JCPND algorithm has been validated by the simulation results of the rate-$1/4$ protograph-based RA codes. Subsequently, a classical protograph code, i.e., the AR3A code, has also been applied to AWGN and ergodic fading channels and has exhibited good error performance [122]. However, the aforementioned works have only provided the simulated error-performance of protograph-based JCPNC schemes without conducting a systematic investigation (e.g., theoretical analysis and design). The main reason is that there is a lack of usable analytical tool for such JCPNC schemes. Although the authors in [156] have proposed an EXIT algorithm for RA-coded JCPNC schemes, the algorithm is not applicable to protograph code because the algorithm is based on the degree-distribution pair of codes.

In the following, we propose a joint finite-length EXIT algorithm for analyzing the protograph-based JCPNC under standard JCPND, in which the MI is traced on each edge of the protograph.

We consider a JCPNC-aided two-way relay channel which comprises two sources A, B, and one relay R. A and B are to exchange message with the help of R. Assuming that the two sources exploit the same protograph code of length N, i.e., $C_{\rm A} = C_{\rm B} = (v_{{\rm A/B},1}, v_{{\rm A/B},2}, \ldots, v_{{\rm A/B},N})$, to encode the source information. The transmission scheme for JCPNC includes two stages: In the 1st stage, the two sources transmit their corresponding BPSK-modulated signals, i.e., $x_{{\rm A},j} = (-1)^{v_{{\rm A},j}}$ and $x_{{\rm B},j} = (-1)^{v_{{\rm B},j}}$, to R simultaneously. Then, R decodes the XORed message $v_{{\rm R},j} = v_{{\rm A},j} \oplus v_{{\rm B},j}$ and retrieves the corresponding information bit $u_{{\rm R},j}$. In the 2nd stage, $u_{{\rm R},j}$ is re-encoded and broadcasted to A and B. In this subsection, we restrict ourselves to the 1st stage as in [153]–[155]. The received signal at R is given by

$$y_{{\rm R},j} = x_{{\rm A},j} + x_{{\rm B},j} + n_{{\rm R},j}, \tag{18}$$

where $n_{{\rm R},j} \sim \mathcal{N}(0, \sigma_n^2)$ is the Gaussian noise. We also assume that $x_{{\rm R},j} = (-1)^{v_{{\rm R},j}}$ is the BPSK-modulated signal of $v_{{\rm R},j}$.

In the absence of noise, there are three possible values for the received signal, denoted by $\mathbf{s}_j = [x_{{\rm A+B},j} = x_{{\rm A},j} + x_{{\rm B},j} : \ x_{{\rm A/B},j} = \{1, -1\}] = [s_{j,0}, s_{j,1}, s_{j,2}] = [2, 0, -2]$. According to [153], [154], we set the a-priori probability of $s_{j,0}, s_{j,1}$, and $s_{j,2}$ to $1/4, 1/2$, and $1/4$, respectively. Then, the channel initial (probability) message is promptly obtained as $\mathbf{g}_j = [g_{j,0}, g_{j,1}, g_{j,2}]$, where $g_{j,\mu} = \beta \exp(-(y_{{\rm R},j} - s_{j,\mu})^2/(2\sigma_n^2))$, for $\mu = 0, 2$, and $g_{j,\mu} = 2\beta \exp(-y_{{\rm R},j}^2/(2\sigma_n^2))$ otherwise[17]. Here β is a normalization factor to keep $\sum_{\mu=0}^{2} g_{j,\mu} = 1$. Based on the channel initial message $\mathbf{g} = \{\mathbf{g}_j\} = \{\mathbf{g}_1, \mathbf{g}_2, \ldots, \mathbf{g}_N\}$, R can decode the XORed codeword $C_{\rm R} = (v_{{\rm R},1}, v_{{\rm R},2}, \ldots, v_{{\rm R},N})$ by using the JCPND algorithm on an equivalent Tanner graph [153], [154].

Similarly to [156], we define two types of LLRs in protograph-based JCPNC for the joint finite-length EXIT analysis. Given a message of the j-th VN/CN for JCPNC, i.e., $\mathbf{p}_j = [p_{j,0}, p_{j,1}, p_{j,2}]$, the *primary* LLR is defined as $L_j = \ln[\Pr(x_{{\rm R},j} = 1|y_{{\rm R},j})/\Pr(x_{{\rm R},j} = -1|y_{{\rm R},j})] = \ln[(p_{j,0} + p_{j,2})/p_{j,1}]$ while the *secondary* LLR is defined as $\rho_j = \ln[\Pr(x_{{\rm A+B},j} = 2|y_{{\rm R},j})/\Pr(x_{{\rm A+B},j} = -2|y_{{\rm R},j})] = \ln(p_{j,0}/p_{j,2})$. Therefore, the primary and secondary channel LLRs are expressed by $L_{{\rm ch},j} = \ln[(g_{j,0} + g_{j,2})/g_{j,1}]$ and $\rho_{{\rm ch},j} = \ln(g_{j,0}/g_{j,2})$, respectively.

Remark: The major difference between the EXIT for channel coding and joint EXIT for JCPNC is that the former one is only related to the primary LLR, while the latter one is dependent on both the primary LLR and secondary LLR.

For protograph-based JCPNC, one can easily demonstrate that the (output) extrinsic primary LLR values of VND/CND approximately follow a symmetric Gaussian distribution, while the probability density function (PDF) of the extrinsic secondary LLR values of VND/CND is not a Gaussian-like distribution. This conclusion is consistent with that of the RA-coded JCPNC [156]. Consequently, we can evaluate the a-priori primary LLR of an XORed VN/CN as

$$L_{Av/Ac}(i,j) = (\sigma_{Av/Ac,j}^2/2) x_{{\rm R},j} + n_{L,j}, \tag{19}$$

where $n_{L,j} \sim \mathcal{N}(0, \sigma_{Av/Ac,j}^2)$ is the Gaussian-distributed random variable.

To simply the analysis, we assume that the decoder knows the perfect a-priori secondary LLR of an XORed VN/CN as in [156], such that

$$\rho_{Av/Ac}(i,j) = \begin{cases} +\Omega & \text{if } x_{{\rm A+B},j} = 2, \\ 0 & \text{if } x_{{\rm A+B},j} = 0, \\ +\Omega & \text{if } x_{{\rm A+B},j} = -2, \end{cases} \tag{20}$$

where Ω denotes a sufficiently large positive value and is set to 20 in our analysis. This secondary LLR model leads to an upper-bound for the extrinsic MI of VND/CND.

Assuming that a protograph code with an $M \times N$ parity-check matrix $\mathbf{H} = (h_{i,j})$ is used as the channel code of

[17] *Note that* $\mathbf{g}_j = [1/4, 1/2, 1/4]$ if the VN is punctured.

JCPNC, we can plot the finite-length EXIT curves of the VND and CND for the protograph-based JCPND, respectively, as follows.

Calculating the extrinsic MI output from the VND

(1) For a given E_b/N_0, we randomly generate two sequences of information bits for A and B and encode them by the same protograph code. The modulated sequences $\{x_{\mathrm{R},j}\}$ and $\{x_{\mathrm{A+B},j}\}$ are readily formed by using the coded bits $\{v_{\mathrm{A},j}\}$ and $\{v_{\mathrm{B},j}\}$. Then, for $j = 1, 2, \ldots, N$, the channel initial message of $v_{\mathrm{R},j}$ is derived as $\mathbf{g}_j = [g_{j,0}, g_{j,1}, g_{j,2}]$.

(2) For a given average a-priori MI $I_{Av} \in [0, 1]$ for the N XORed VNs, we calculate the variance σ_{Av}^2 of the average a-priori primary LLR using [88, eq.(4)] based on the symmetric Gaussian assumption. Next, for $i = 1, 2, \ldots, M$ and $j = 1, 2, \ldots, N$, we generate the a-priori primary LLR $L_{Av}(i, j)$ and secondary LLR $\rho_{Av}(i, j)$ exploiting (19) and (20), respectively, if $h_{i,j} \neq 0$.

(3) Combining $L_{Av}(i, j)$, $\rho_{Av}(i, j)$, and $\sum_{\mu=0}^{2} p_{Av,\mu}(i, j) = 1$ yields the corresponding a-priori message $\mathbf{p}_{Av}(i, j) = [p_{Av,0}(i, j), p_{Av,1}(i, j), p_{Av,2}(i, j)]$.

(4) The sequences $\{\mathbf{g}_j\}$ and $\{\mathbf{p}_{Av}(i, j)\}$ are passed through the VND to become the sequence of extrinsic message $\{\mathbf{p}_{Ev}(i, j)\}$. The relationship among them can be expressed as $\mathbf{p}_{Ev}(i, j) = F_{\mathrm{VND}}(\mathbf{g}_j, \mathbf{p}_{Av}(i, j))$, where F_{VND} represents the probability-message processor of VND.

(5) For $i = 1, 2, \ldots, M$ and $j = 1, 2, \ldots, N$, we can easily obtain the extrinsic primary LLR $L_{Ev}(i, j)$ based on $\mathbf{p}_{Ev}(i, j)$ if $h_{i,j} \neq 0$. Further, the average extrinsic MI corresponding to the sequence $\{L_{Ev}(i, j)\}$ is evaluated as [17]

$$I_{Ev} = \frac{1}{2} \sum_{\tau=\{-1,1\}} \int_{-\infty}^{\infty} f_{Ev}(\xi | X_{\mathrm{R},j} = \tau) \times \log_2 \frac{2 f_{Ev}(\xi | X_{\mathrm{R},j} = \tau)}{f_{Ev}(\xi | X_{\mathrm{R},j} = -1) + f_{Ev}(\xi | X_{\mathrm{R},j} = 1)} d\xi, \tag{21}$$

where $f_{Ev}(\xi | X_{\mathrm{R},j} = \tau)$ is the conditional PDF of sequence $\{L_{Ev}(i, j)\}$ given $X_{\mathrm{R},j} = \tau$.

(6) Repeat Steps 1 $\sim$ 5 to obtain a sufficient set of I_{Ev} values. We then calculate the mean and variance of I_{Ev} as $\mathbb{E}[I_{Ev}]$ and $\mathrm{var}[I_{Ev}]$, respectively. In particular, the mean value $\mathbb{E}[I_{Ev}]$ is considered as a typical MI value for all the finite-length codewords.

(7) Execute Steps 1 $\sim$ 6 for different values of $I_{Av} \in [0, 1]$ to get an EXIT band for VND, which includes an expected EXIT curve $(I_{Av}, \mathbb{E}[I_{Ev}])$, an upper-bound curve $(I_{Av}, \mathbb{E}[I_{Ev}] + 3\sqrt{\mathrm{var}[I_{Ev}]})$, and a lower-bound curve $(I_{Av}, \mathbb{E}[I_{Ev}] - 3\sqrt{\mathrm{var}[I_{Ev}]})$.

Calculating the extrinsic MI output from the CND

Likewise, one can also obtain an EXIT band for the CND through a similar way. We represent the expected EXIT curve, upper-bound curve, and lower-bound curve of the CND as $(I_{Ac}, \mathbb{E}[I_{Ec}])$, $(I_{Ac}, \mathbb{E}[I_{Ec}] + 3\sqrt{\mathrm{var}[I_{Ec}]})$, and $(I_{Ac}, \mathbb{E}[I_{Ec}] - 3\sqrt{\mathrm{var}[I_{Ec}]})$, respectively.

Based on the aforementioned description, the block diagram of the finite-length EXIT algorithm for the protograph-based JCPND is shown as Fig. 25, where "MPC" and "PMC" are used to denote the "MI-to-probability-message converter" and "probability-message-to-MI converter", respectively. Furthermore, the MPC and PMC are implemented by Steps 2 $\sim$ 3 and Step 5, respectively.

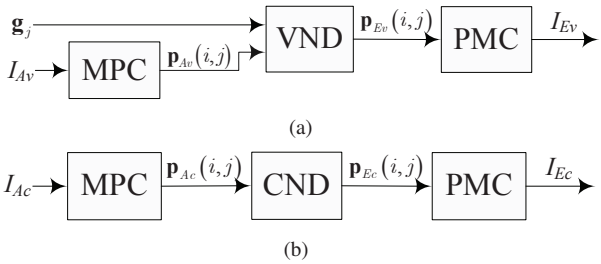

Fig. 25. Block diagram of the finite-length EXIT algorithm for the protograph-based JCPND. (a) Calculation of the extrinsic MI output from the VND and (b) calculation of the extrinsic MI output from the CND.

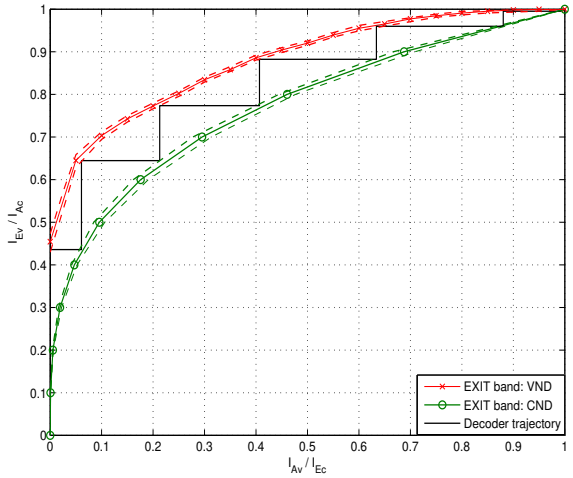

Fig. 26. EXIT bands and actual decoding trajectory of the AR3A-coded JCPNC scheme in an AWGN channel. The expected EXIT curves are denoted by the solid lines while the upper-bound curves and lower-bound curves are denoted by the dotted lines. The parameters used are $R = 1/2$, $K = 1536$, and $E_b/N_0 = 2.8$ dB.

Remark: The EXIT band of VND is related to E_b/N_0 since it is directly connected to the channel, while the EXIT band of CND is independent of E_b/N_0.

Example 11: Consider a rate-$1/2$ AR3A code with information length $K = 1536$, we plot the EXIT bands and actual decoding trajectory of the protograph-based JCPNC scheme in an AWGN channel at $E_b/N_0 = 2.8$ dB in Fig. 26. We observe that the EXIT bands can characterize the decoding trajectory with reasonable accuracy. We also present the simulated BER curves of the JCPNC schemes based on the rate-$1/2$ AR3A code and $(3, 6)$ regular LDPC code with information length $K = 1536$ in an AWGN channel in Fig. 27. The results indicate that the AR3A-coded JCPNC is remarkably superior to the regular-coded one and exhibits excellent error performance.

2) Protograph-based JCPNC in fading channels: Besides the research in AWGN channels, the protograph-based JCPNC has been considered under fading condition in [123]. In that work, the interplay between the protograph-based JCPNC and space-time block coding has been studied in ergodic fading channels. To tackle the JCPND of the combined framework,

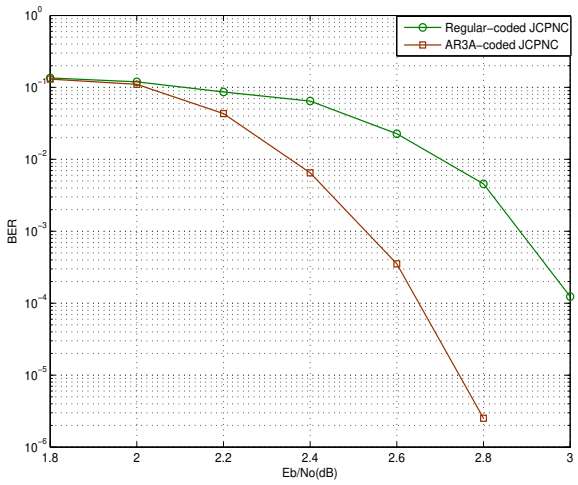

Fig. 27. Simulated BER curves of the AR3A-coded and the regular-coded JCPNC schemes in an AWGN channel. The parameters used are $R = 1/2$ and $K = 1536$.

a novel precoding scheme has been proposed and a simplified updating rule of LLR in the JCPND algorithm has been developed. Moreover, the corresponding asymptotic BER formula has been derived and will be useful for the design of protograph-based JCPNC schemes in such channels.

However, thus far, there is no related work on optimizing protograph codes for JCPNC schemes in neither AWGN nor fading channels.

C. Conclusion

In this section, we have introduced two attractive applications of protograph codes, namely the protograph-based JSCC and protograph-based JCPNC. We have first summarized the state-of-the-art in protograph-based JSCC schemes in Sect. V-A. Afterwards, we have concluded the achievement of protograph-based JCPNC schemes in Sect. V-B. Moreover, a novel joint finite-length EXIT algorithm has been proposed in the same subsection to analyze the convergence performance of protograph-based JCPNC schemes in AWGN channels. The algorithm should therefore facilitate the related design work.

VI. Concluding Remarks and Future Lines

A. Concluding Remarks

In this treatise, we have conducted an insightful survey of the associated literature, which is related to the protograph codes and their applications. We have considered the design and analysis aspects of such codes in various transmission scenarios and their meritorious variants, as well as their applications to JSCC and JCPNC. We have limited our elaboration to the encoding design and assumed that the decoder was implemented by the BP algorithm.

To be specific, we have firstly presented the background of LDPC codes, the basic principles of protograph codes as well as their analytical methodologies. Then, we have provided the corresponding guidelines for the design of good fixed-rate and RC protograph codes, which possess both fundamental-limit-approaching error performance and linear-minimum-distance property, in AWGN channels, ergodic fading channels, non-ergodic BF channels, PR channels, and Poisson PPM channels, respectively. The results have indicated that the designed protograph codes exhibit more excellent performance with respect to existing counterparts in the above-mentioned channels.

In addition to the design and analysis aspects, the applications of protograph codes to JSCC and JCPNC frameworks have been extensively discussed in both AWGN and ergodic fading channels. Particularly, a novel joint finite-length EXIT algorithm has been developed for protograph-based JCPNC systems in AWGN channels. The algorithm can be considered as an efficient theoretical tool for the optimization of such systems.

In general, the protograph codes have shown their superiorities for use in a variety of communication and data storage systems, such as deep-space communication systems, wireless communication systems, and magnetic recording systems. Also, this type of codes possesses some promising characteristics to become a good candidate for JSCC and JCPNC.

B. Future Lines

This paper has offered an overall review of the research progress of protograph codes since the invention of them. This type of codes has already proposed for the next generation uplink standard of the Consultative Committee for Space Data Systems due to the excellent performance and low complexity. Beyond any doubt, protograph codes may find more employment in a significant amount of other potential applications and be included in other new standards in the future. Nonetheless, the study on protograph codes was launched in 2003 and this type of codes has just been undergoing development in recent ten years, there exist various open problems that need to be addressed. Some of them are listed as follows.

1) As mentioned in Sect. II and Sect. III, non-binary protograph codes have been introduced in AWGN channels [66]. The non-binary protograph codes can outperform their binary counterparts in some cases and are more easily combined with high-order modulations. Accordingly, a strong focus on extending the design of protograph codes to the non-binary domain in other types of channels, e.g., ergodic/non-ergodic fading channels, is certainly to be expected.
2) Although the performance of protograph codes has been well investigated in point-to-point, SIMO, and relay fading channels, these architectures may not be enough to satisfy the requirement of the modern wireless communications. One of the ambitious goals of the next-generation (5G) wireless communication systems is to reliably provide very high data-rate transmission to multiple users simultaneously. Hence, the design of protograph codes for multiple-input multiple-output (MIMO) systems, which are considered as a critical technique for 5G, will be much appreciated.
3) To overcome the limitation of storage density in conventional data storage systems, bit-patterned media has been proposed [157]–[159]. Unfortunately, this results in severe inter-track interference and the corresponding system

should be re-described as a two-dimensional PR channel, which comprises both ISI and inter-track interference. Till now, the protograph codes have been successfully optimized for one-dimensional PR channels, but their performance in two-dimensional PR channels is not well understood and can be served as a future line.

4) FEC is a key enabling technique for the next-generation optical communication systems. As a type of superior FEC codes, LDPC codes have been widely used in such systems [37], [160]. Since protograph codes can accomplish capacity-approaching performance with high code rate (i.e, $R \geq 4/5$), which fits well with the requirement for optical communication systems, they have potential to become an efficient solution to realize reliable communication in optical transport networks.
5) According to Sect. V, the construction and analytical methodologies of protograph-based JSCC and JCPNC have been proposed for several channel conditions. Further development on the aforementioned two areas will focus on the optimization of protograph-based JSCC and JCPNC using the joint EXIT-chart-based methods so as to approach their corresponding capacities, respectively.
6) Finally, we anticipate that another potential research area is systematic study of the variants of protograph codes. For example, as a rateless relative of protograph codes, PBRL codes have been proposed recently [75], which have a similar structure to the Raptor codes. Rateless codes, e.g., Raptor codes [161], provide a more flexible way for channel coding and are very suitable for scenarios where channel state information is unavailable at the transmitter terminal. Therefore, more effort may be devoted to in-depth investigation on the existing variants of protograph codes as well as developing other new meritorious variants in the near future.

REFERENCES

[1] D. J. Costello and G. D. Forney, "Channel coding: The road to channel capacity," *Proc. IEEE*, vol. 95, no. 6, pp. 1150–1177, Jun. 2007.

[2] C. E. Shannon, "A mathematical theory of communication," *Bell Syst. Tech. J.*, vol. 27, pp. 379–423, Jul. 1948.

[3] R. W. Hamming, "Error detecting and error correcting codes," *Bell Syst. Tech. J.*, vol. 29, pp. 147–160, Apr. 1950.

[4] R. G. Gallager, *Low-Density Parity-Check Codes*. Cambridge, MA: MIT Press, 1963.

[5] R. M. Tanner, "A recursive approach to low complexity codes," *IEEE Trans. Inf. Theory*, vol. 27, no. 5, pp. 533–547, Sept. 1981.

[6] C. Berrou, A. Glavieux, and P. Thitimajshima, "Near Shannon limit error-correcting coding and decoding: Turbo-codes," in *Proc. IEEE Int. Conf. Commun. (ICC)*, vol. 2, May 1993, pp. 1064–1070.

[7] D. J. MacKay and R. M. Neal, "Good codes based on very sparse matrices," in *Proc. Cryptography and Coding. 5th IMA Conf., number 1025 in Lecture Notes in Comput. Sci.*, Oct. 1995, pp. 100–111.

[8] N. Alon and M. Luby, "A linear time erasure-resilient code with nearly optimal recovery," *IEEE Trans. Inf. Theory*, vol. 42, no. 6, pp. 1732–1736, Nov. 1996.

[9] M. Sipser and D. Spielman, "Expander codes," *IEEE Trans. Inf. Theory*, vol. 42, no. 6, pp. 1710–1722, Nov. 1996.

[10] D. J. C. MacKay and R. M. Neal, "Near Shannon limit performance of low density parity check codes," *Electron. Lett.*, vol. 33, no. 6, pp. 457–458, Mar. 1997.

[11] D. J. C. MacKay, "Good error-correcting codes based on very sparse matrices," *IEEE Trans. Inf. Theory*, vol. 45, no. 2, pp. 399–431, Mar. 1999.

[12] T. Richardson and R. Urbanke, "The capacity of low-density parity-check codes under message-passing decoding," *IEEE Trans. Inf. Theory*, vol. 47, no. 2, pp. 599–618, Feb. 2001.

[13] T. Richardson, M. Shokrollahi, and R. Urbanke, "Design of capacity-approaching irregular low-density parity-check codes," *IEEE Trans. Inf. Theory*, vol. 47, no. 2, pp. 619–637, Feb. 2001.

[14] M. G. Luby, M. Mitzenmacher, M. A. Shokrollahi, D. A. Spielman, and V. Stemann, "Practical loss-resilient codes," in *Proc. 29th Annual ACM Symp. Theory of Comput.*, May 1997, pp. 150–159.

[15] D. Spielman, "Linear-time encodable and decodable error-correcting codes," *IEEE Trans. Inf. Theory*, vol. 42, no. 6, pp. 1723–1731, Nov. 1996.

[16] T. Richardson and R. Urbanke, "Efficient encoding of low-density parity-check codes," *IEEE Trans. Inf. Theory*, vol. 47, no. 2, pp. 638–656, Feb. 2001.

[17] S. ten Brink, "Convergence behavior of iteratively decoded parallel concatenated codes," *IEEE Trans. Commun.*, vol. 49, no. 10, pp. 1727–1737, Oct. 2001.

[18] S. ten Brink, G. Kramer, and A. Ashikhmin, "Design of low-density parity-check codes for modulation and detection," *IEEE Trans. Commun.*, vol. 52, no. 4, pp. 670–678, Apr. 2004.

[19] A. Ashikhmin, G. Kramer, and S. ten Brink, "Extrinsic information transfer functions: Model and erasure channel properties," *IEEE Trans. Inf. Theory*, vol. 50, no. 11, pp. 2657–2673, Nov. 2004.

[20] M. Franceschini, G. Ferrari, and R. Raheli, "Does the performance of LDPC codes depend on the channel?" *IEEE Trans. Commun.*, vol. 54, no. 12, pp. 2129–2132, Dec. 2006.

[21] F. Peng, W. Ryan, and R. Wesel, "Surrogate-channel design of universal LDPC codes," *IEEE Commun. Lett.*, vol. 10, no. 6, pp. 480–482, Jun. 2006.

[22] H. Xiao and A. Banihashemi, "Improved progressive-edge-growth (PEG) construction of irregular LDPC codes," *IEEE Commun. Lett.*, vol. 8, no. 12, pp. 715–717, Dec. 2004.

[23] X.-Y. Hu, E. Eleftheriou, and D.-M. Arnold, "Regular and irregular progressive edge-growth tanner graphs," *IEEE Trans. Inf. Theory*, vol. 51, no. 1, pp. 386–398, Jan. 2005.

[24] G. Richter and A. Hof, "On a construction method of irregular LDPC codes without small stopping sets," in *Proc. IEEE Int. Conf. Commun.*, vol. 3, Jun. 2006, pp. 1119–1124.

[25] X. Zheng, F. C. M. Lau, and C. K. Tse, "Constructing short-length irregular LDPC codes with low error floor," *IEEE Trans. Commun.*, vol. 58, no. 10, pp. 2823–2834, Oct. 2010.

[26] N. Bonello, S. Chen, and L. Hanzo, "Low-density parity-check codes and their rateless relatives," *IEEE Commun. Surveys & Tutorials*, vol. 13, no. 1, pp. 3–26, First Quarter 2011.

[27] J. M. F. Moura, J. Lu, and H. Zhang, "Structured low-density parity-check codes," *IEEE Signal Process. Mag.*, vol. 21, no. 1, pp. 42–55, Jan. 2004.

[28] G. Liva, S. Song, L. Lan, Y. Zhang, W. Ryan, and S. Lin, "Design of LDPC codes: A survey and new results," *J. Commun. Softw. Syst.*, vol. 2, no. 3, pp. 191–211, Sept. 2006.

[29] M. El-Hajjar and L. Hanzo, "EXIT charts for system design and analysis," *IEEE Commun. Surveys & Tutorials*, vol. 16, no. 1, pp. 127–153, First Quarter 2014.

[30] M. Yazdani, S. Hemati, and A. Banihashemi, "Improving belief propagation on graphs with cycles," *IEEE Commun. Lett.*, vol. 8, no. 1, pp. 57–59, Jan. 2004.

[31] M.-H. Taghavi and P. Siegel, "Adaptive methods for linear programming decoding," *IEEE Trans. Inf. Theory*, vol. 54, no. 12, pp. 5396–5410, Dec. 2008.

[32] N. Varnica, M. Fossorier, and A. Kavcic, "Augmented belief propagation decoding of low-density parity check codes," *IEEE Trans. Commun.*, vol. 55, no. 7, pp. 1308–1317, Jul. 2007.

[33] Y. Fang, J. Zhang, L. Wang, and F. C. M. Lau, "BP-Maxwell decoding algorithm for LDPC codes over AWGN channels," in *Proc. 6th Int. Conf. Wireless Commun. Netw. and Mobile Comput. (WiCOM)*, Sept. 2010, pp. 1–4.

[34] K. Andrews, D. Divsalar, S. Dolinar, J. Hamkins, C. Jones, and F. Pollara, "The development of turbo and LDPC codes for deep-space applications," *Proc. IEEE*, vol. 95, no. 11, pp. 2142–2156, Nov. 2007.

[35] G. Calzolari, M. Chiani, F. Chiaraluce, R. Garello, and E. Paolini, "Channel coding for future space missions: New requirements and trends," *Proc. IEEE*, vol. 95, no. 11, pp. 2157–2170, Nov. 2007.

[36] J. Hou, P. Siegel, and L. Milstein, "Performance analysis and code optimization of low density parity-check codes on Rayleigh fading channels," *IEEE J. Sel. Areas Commun.*, vol. 19, no. 5, pp. 924–934, May 2001.

[37] I. Djordjevic, "On the irregular nonbinary QC-LDPC-coded hybrid multidimensional OSCD-modulation enabling beyond 100 Tb/s optical transport," *J. Lightwave Technol.*, vol. 31, no. 16, pp. 2669–2675, Aug. 2013.

[38] H. Song, R. Todd, and J. Cruz, "Low density parity check codes for magnetic recording channels," *IEEE Trans. Magn.*, vol. 36, no. 5, pp. 2183–2186, Sept. 2000.

[39] B. Kurkoski, P. Siegel, and J. Wolf, "Joint message-passing decoding of LDPC codes and partial-response channels," *IEEE Trans. Inf. Theory*, vol. 48, no. 6, pp. 1410–1422, Jun. 2002.

[40] S. Lin and D. J. Costello, *Error Control Coding: Fundamentals and Applications, Second Edition*. Upper Saddle River, NJ, USA: Prentice-Hall, 2004.

[41] W. E. Ryan, "An introduction to LDPC codes," *CRC Handbook for Coding and Signal Process. for Recording Syst.*, 2004.

[42] T. Richardson and R. Urbanke, "The renaissance of Gallager's low-density parity-check codes," *IEEE Commun. Mag.*, vol. 41, no. 8, pp. 126–131, Aug. 2003.

[43] ——, *Modern Coding Theory*. Cambridge, U.K.: Cambridge University Press, 2008.

[44] F. Kschischang, "Codes defined on graphs," *IEEE Commun. Mag.*, vol. 41, no. 8, pp. 118–125, Aug. 2003.

[45] M. Fossorier, "Quasi-cyclic low-density parity-check codes from circulant permutation matrices," *IEEE Trans. Inf. Theory*, vol. 50, no. 8, pp. 1788–1793, Aug. 2004.

[46] T. Richardson and R. Urbanke, "Multi-edge type LDPC codes," *Presented at the Workshop honoring Prof. Bob McEliece on his 60th birthday*, California Institute of Technology, May 2002. [Online]. Available: http://citeseerx.ist.psu.edu/viewdoc/summary?doi=10.1.1.106.7310

[47] J. Thorpe, "Low-density parity-check (LDPC) codes constructed from protographs," in *Proc. IPN Progress Report*, Aug. 2003, pp. 1–7.

[48] D. Divsalar, C. Jones, S. Dolinar, and J. Thorpe, "Protograph based LDPC codes with minimum distance linearly growing with block size," in *Proc. IEEE Global Commun. Conf. (GLOBECOM)*, vol. 3, Nov. 2005.

[49] A. Abbasfar, D. Divsalar, and K. Yao, "Accumulate-repeat-accumulate codes," *IEEE Trans. Commun.*, vol. 55, no. 4, pp. 692–702, Apr. 2007.

[50] D. Divsalar, S. Dolinar, C. Jones, and K. Andrews, "Capacity-approaching protograph codes," *IEEE J. Sel. Areas Commun.*, vol. 27, no. 6, pp. 876–888, Aug. 2009.

[51] S. Abu-Surra, D. Divsalar, and W. Ryan, "On the existence of typical minimum distance for protograph-based LDPC codes," in *Proc. IEEE Inf. Theory and Applications Workshop (ITA)*, Jan. 2010, pp. 1–7.

[52] ——, "Enumerators for protograph-based ensembles of LDPC and generalized LDPC codes," *IEEE Trans. Inf. Theory*, vol. 57, no. 2, pp. 858–886, Feb. 2011.

[53] M. Lentmaier and K. S. Zigangirov, "On generalized low-density parity-check codes based on Hamming component codes," *IEEE Commun. Lett.*, vol. 3, no. 8, pp. 248–250, Aug 1999.

[54] S. Abu-Surra, G. Liva, and W. Ryan, "Design and performance of selected classes of Tanner codes," in *Proc. UCSD Workshop on Inf. Theory and its Applications (ITA)*, Feb. 2006, pp. 6–10.

[55] G. Liva, W. E. Ryan, and M. Chiani, "Design of quasi-cyclic Tanner codes with low error floors," in *Proc. Int. Symp. Turbo Codes Related Topics (ISTC)*, Apr. 2006, pp. 1–6.

[56] S. Abu-Surra, G. Liva, and W. E. Ryan, "Low-floor Tanner codes via Hamming-node or RSCC-node doping," in *Proc. Int. Symp. Applied Algebra, Algebraic Algorithms and Error-Correcting Codes*, Feb. 2006, pp. 245–254.

[57] G. Liva, W. E. Ryan, and M. Chiani, "Quasi-cyclic generalized LDPC codes with low error floors," *IEEE Trans. Commun.*, vol. 55, no. 12, pp. 2381–2381, Dec. 2007.

[58] G. Liva and M. Chiani, "Protograph LDPC codes design based on EXIT analysis," in *Proc. IEEE Global Commun. Conf. (GLOBECOM)*, Nov. 2007, pp. 3250–3254.

[59] S. Dolinar, "A rate-compatible family of protograph-based LDPC codes built by expurgation and lengthening," in *Proc. IEEE Int. Symp. Inf. Theory (ISIT)*, Sept. 2005, pp. 1627–1631.

[60] M. El-Khamy, J. Hou, and N. Bhushan, "Design of rate-compatible structured LDPC codes for hybrid ARQ applications," *IEEE J. Sel. Areas Commun.*, vol. 27, no. 6, pp. 965–973, Aug. 2009.

[61] T. Nguyen, A. Nosratinia, and D. Divsalar, "The design of rate-compatible protograph LDPC codes," *IEEE Trans. Commun.*, vol. 60, no. 10, pp. 2841–2850, Oct. 2012.

[62] T. V. Nguyen and A. Nosratinia, "Rate-compatible short-length protograph LDPC codes," *IEEE Commun. Lett.*, vol. 17, no. 5, pp. 948–951, May 2013.

[63] M. Davey and D. MacKay, "Low-density parity check codes over GF(q)," *IEEE Commun. Lett.*, vol. 2, no. 6, pp. 165–167, Jun. 1998.

[64] J. Huang, L. Liu, W. Zhou, and S. Zhou, "Large-girth nonbinary QC-LDPC codes of various lengths," *IEEE Trans. Commun.*, vol. 58, no. 12, pp. 3436–3447, Dec. 2010.

[65] G. Han, Y. L. Guan, and X. Huang, "Check node reliability-based scheduling for BP decoding of non-binary LDPC codes," *IEEE Trans. Commun.*, vol. 61, no. 3, pp. 877–885, Mar. 2013.

[66] B.-Y. Chang, L. Dolecek, and D. Divsalar, "EXIT chart analysis and design of non-binary protograph-based LDPC codes," in *Proc. Military Commun. Conf. (MILCOM)*, Nov. 2011, pp. 566–571.

[67] L. Costantini, B. Matuz, G. Liva, E. Paolini, and M.Chiani, "Non-binary protograph LDPC codes for space communications," *Int. J. Sat. Commun. Netw.*, vol. 30, no. 2, pp. 43–51, Mar 2012.

[68] D. Divsalar and L. Dolecek, "On the typical minimum distance of protograph-based non-binary LDPC codes," in *Proc. Inf. Theory and Applications Workshop (ITA)*, Feb. 2012, pp. 192–198.

[69] L. Dolecek, D. Divsalar, Y. Sun, and B. Amiri, "Non-binary protograph-based LDPC codes: Enumerators, analysis, and designs," *IEEE Trans. Inf. Theory*, vol. 60, no. 7, pp. 3913–3941, Jul. 2014.

[70] A. J. Felstrom and K. Zigangirov, "Time-varying periodic convolutional codes with low-density parity-check matrix," *IEEE Trans. Inf. Theory*, vol. 45, no. 6, pp. 2181–2191, Sept. 1999.

[71] D. Mitchell, A. Pusane, K. Zigangirov, and D. Costello, "Asymptotically good LDPC convolutional codes based on protographs," in *Proc. IEEE Int. Symp. Inf. Theory (ISIT)*, Jul. 2008, pp. 1030–1034.

[72] D. Mitchell, A. Pusane, N. Goertz, and D. Costello, "Free distance bounds for protograph-based regular LDPC convolutional codes," in *Proc. Int. Symp. Turbo Codes and Related Topics (ISTC)*, Sept. 2008, pp. 408–413.

[73] D. Mitchell, A. Pusane, and D. Costello, "Minimum distance and trapping set analysis of protograph-based LDPC convolutional codes," *IEEE Trans. Inf. Theory*, vol. 59, no. 1, pp. 254–281, Jan. 2013.

[74] T.-Y. Chen, D. Divsalar, and R. Wesel, "Protograph-based Raptor-like LDPC codes with low thresholds," in *Proc. IEEE Int. Conf. Commun. (ICC)*, Jun. 2012, pp. 2161–2165.

[75] T.-Y. Chen, D. Divsalar, J. Wang, and R. Wesel, "Protograph-based Raptor-like LDPC codes for rate compatibility with short block-lengths," in *Proc. IEEE Global Telecommun. Conf. (GLOBECOM)*, Dec. 2011, pp. 1–6.

[76] T.-Y. Chen, K. Vakilinia, D. Divsalar, and R. Wesel, "Protograph-based Raptor-like LDPC codes," Mar. 2014. [Online]. Available: http://arxiv.org/pdf/1403.2111v1.pdf

[77] H. Uchikawa, K. Kasai, and K. Sakaniwa, "Spatially coupled LDPC codes for decode-and-forward in erasure relay channel," in *Proc. IEEE Int. Symp. Inf. Theory (ISIT)*, Jul. 2011, pp. 1474–1478.

[78] L. Wei, D. J. Costello, and T. E. Fuja, "Coded cooperation using rate-compatible spatially-coupled codes," in *Proc. IEEE Int. Symp. Inf. Theory (ISIT)*, Jul. 2013, pp. 1869–1873.

[79] N. Bonello, S. Chen, and L. Hanzo, "Construction of regular quasi-cyclic protograph LDPC codes based on Vandermonde matrices," *IEEE Trans. Veh. Technol.*, vol. 57, no. 4, pp. 2583–2588, Jul. 2008.

[80] M. Karimi and A. Banihashemi, "On the girth of quasi-cyclic protograph LDPC codes," *IEEE Trans. Inf. Theory*, vol. 59, no. 7, pp. 4542–4552, Jul. 2013.

[81] Q. Huang, Q. Diao, S. Lin, and K. Abdel-Ghaffar, "Cyclic and quasi-cyclic LDPC codes on constrained parity-check matrices and their trapping sets," *IEEE Trans. Inf. Theory*, vol. 58, no. 5, pp. 2648–2671, May 2012.

[82] V. Nguyen, "Design of Capacity-approaching Protograph-based LDPC Coding Systems," Ph.D. dissertation, University of Texas at Dallas, Dallas, TX, Dec. 2012.

[83] S. Yang, L. Wang, Y. Fang, and P. Chen, "Performance of improved AR3A code over EPR4 channel," in *Proc. Int. Conf. Comput. Research and Development (ICCRD)*, vol. 2, Mar. 2011, pp. 60–64.

[84] J. Li and K. R. Narayanan, "Rate-compatible low density parity check codes for capacity-approaching ARQ schemes in packet data communications," in *Proc. Int. Conf. Commun., Internet, and Inf. Technol. (CIIT)*, Nov. 2002, pp. 201–206.

[85] S.-Y. Chung, "On the construction of some capacity-approaching coding schemes," Ph.D. dissertation, Massachusetts Institute of Technology, Cambridge, MA, Sept. 2000.

[86] C. Di, D. Proietti, I. Telatar, T. Richardson, and R. Urbanke, "Finite-length analysis of low-density parity-check codes on the binary erasure channel," *IEEE Trans. Inf. Theory*, vol. 48, no. 6, pp. 1570–1579, Jun. 2002.

[87] P. Tan and J. Li, "Finite-length extrinsic information transfer (EXIT) analysis for coded and precoded ISI channels," *IEEE Trans. Magn.*, vol. 44, no. 5, pp. 648–655, May 2008.

[88] Y. Fang, P. Chen, L. Wang, and F. C. M. Lau, "Design of protograph LDPC codes for partial response channels," *IEEE Trans. Commun.*, vol. 60, no. 10, pp. 2809–2819, Oct. 2012.

[89] T. M. Cover and J. A. Thomas, *Elements of Information Theory*. New York, NY, USA: John Wiley & Sons, 1991.

[90] D. J. C. MacKay and M. S. Postol, "Weaknesses of Margulis and Ramanujan-Margulis low-density parity-check codes," *Electron. Notes Theor. Comput. Sci.*, vol. 74, pp. 97–104, 2003.

[91] S. Litsyn and V. Shevelev, "Distance distributions in ensembles of irregular low-density parity-check codes," *IEEE Trans. Inf. Theory*, vol. 49, no. 12, pp. 3140–3159, Dec. 2003.

[92] ——, "On ensembles of low-density parity-check codes: asymptotic distance distributions," *IEEE Trans. Inf. Theory*, vol. 48, no. 4, pp. 887–908, Apr. 2002.

[93] A. Orlitsky, K. Viswanathan, and J. Zhang, "Stopping set distribution of LDPC code ensembles," *IEEE Trans. Inf. Theory*, vol. 51, no. 3, pp. 929–953, Mar. 2005.

[94] D. Divsalar, S. Dolinar, and C. Jones, "Construction of protograph LDPC codes with linear minimum distance," in *Proc. IEEE Int. Symp. Inf. Theory (ISIT)*, Jul. 2006, pp. 664–668.

[95] B. K. Butler and P. H. Siegel, "On distance properties of quasi-cyclic protograph-based LDPC codes," in *Proc. IEEE Int. Symp. Inf. Theory (ISIT)*, Jun. 2010, pp. 809–813.

[96] D. Divsalar and C. Jones, "Protograph LDPC codes with node degrees at least 3," in *Proc. IEEE Global Telecommun. Conf. (GLOBECOM)*, Nov. 2006, pp. 1–5.

[97] S. Abu-Surra, W. Ryan, and D. Divsalar, "Ensemble enumerators for protograph-based generalized LDPC codes," in *Proc. IEEE Global Telecommun. Conf. (GLOBECOM)*, Nov. 2007, pp. 1492–1497.

[98] A. Abbasfar, D. Divsalar, and K. Yao, "Accumulate repeat accumulate codes," in *Proc. IEEE Global Telecommun. Conf. (GLOBECOM)*, vol. 1, Nov. 2004, pp. 509–513.

[99] D. Divsalar, S. Dolinar, and J. Thorpe, "Accumulate-repeat-accumulate-accumulate-codes," in *Proc. IEEE 60th Veh. Technol. Conf. (VTC)*, vol. 3, Sept. 2004, pp. 2292–2296.

[100] D. Divsalar, S. Dolinar, and C. Jones, "Low-rate LDPC codes with simple protograph structure," in *Proc. IEEE Int. Symp. Inf. Theory (ISIT)*, Sept. 2005, pp. 1622–1626.

[101] T. V. Nguyen, A. Nosratinia, and D. Divsalar, "Bilayer protograph codes for half-duplex relay channels," in *Proc. IEEE Int. Symp. Inf. Theory (ISIT)*, Jun. 2010, pp. 948–952.

[102] ——, "Bilayer protograph codes for half-duplex relay channels," *IEEE Trans. Wireless Commun.*, vol. 12, no. 5, pp. 1969–1977, May 2013.

[103] H. Zhou, M. Jiang, C. Zhao, and J. Wang, "Optimization of protograph-based LDPC coded BICM-ID for the Poisson PPM channel," *IEEE Commun. Lett.*, vol. 17, no. 12, pp. 2344–2347, Dec. 2013.

[104] C. A. Kelley, "Algebraic design and implementation of protograph codes using non-commuting permutation matrices," *IEEE Trans. Commun.*, vol. 61, no. 3, pp. 910–918, Mar. 2013.

[105] A. R. Iyengar, M. Papaleo, P. Siegel, J. Wolf, A. Vanelli-Coralli, and G. Corazza, "Windowed decoding of protograph-based LDPC convolutional codes over erasure channels," *IEEE Trans. Inf. Theory*, vol. 58, no. 4, pp. 2303–2320, Apr. 2012.

[106] T. V. Nguyen, A. Nosratinia, and D. Divsalar, "Threshold of protograph-based LDPC coded BICM for Rayleigh fading," in *Proc. IEEE Global Telecommun. Conf. (GLOBECOM)*, Dec. 2011, pp. 1–5.

[107] Y. Fang, P. Chen, L. Wang, F. C. M. Lau, and K.-K. Wong, "Performance analysis of protograph-based low-density parity-check codes with spatial diversity," *IET Commun.*, vol. 6, no. 17, pp. 2941–2948, Nov. 2012.

[108] Y. Fang, K.-K. Wong, L. Wang, and K.-F. Tong, "Performance analysis of protograph low-density parity-check codes for Nakagami-m fading relay channels," *IET Commun.*, vol. 7, no. 11, pp. 1133–1139, Jul. 2013.

[109] P. Pulini, G. Liva, and M. Chiani, "Protograph EXIT analysis over block fading channels with application to relays," in *Proc. IEEE Int. Conf. Commun. (ICC)*, Jun. 2012, pp. 4728–4733.

[110] ——, "Unequal diversity LDPC codes for relay channels," *IEEE Trans. Wireless Commun.*, vol. 12, no. 11, pp. 5646–5655, Nov. 2013.

[111] Y. Fang, G. Bi, and Y. L. Guan, "Design and analysis of root-protograph LDPC codes for non-ergodic block-fading channels," *IEEE Trans. Wireless Commun.*, vol. 14, no. 2, pp. 738–749, Feb. 2015.

[112] Y. Fang, Y. L. Guan, G. Bi, L. Wang, and F. C. M. Lau, "Rate-compatible root-protograph LDPC codes for quasi-static fading relay channels," accepted for publication, *IEEE Trans Veh. Technol.*, Mar. 2015.

[113] P. Grosa, A. F. dos Santos, M. Lentmaier, W. Rave, and G. Fettweis, "Application of protograph-based LDPC codes for UWB short range communication," in *Proc. IEEE Int. Conf. Ultra-Wideband (ICUWB)*, vol. 2, Sept. 2010, pp. 1–4.

[114] T. Van Nguyen, A. Nosratinia, and D. Divsalar, "Protograph-based LDPC codes for partial response channels," in *Proc. IEEE Int. Conf. Commun. (ICC)*, Jun. 2012, pp. 2166–2170.

[115] T. V. Nguyen, A. Nosratinia, and D. Divsalar, "Rate-compatible protograph-based LDPC codes for inter-symbol interference channels," *IEEE Commun. Lett.*, vol. 17, no. 8, pp. 1632–1635, Aug. 2013.

[116] W. Phakphisut, P. Supnithi, and N. Puttarak, "EXIT chart analysis of nonbinary protograph LDPC codes for partial response channels," *IEEE Trans. Magn.*, vol. 50, no. 11, pp. 1–4, Nov. 2014.

[117] J. He, L. Wang, and P. Chen, "A joint source and channel coding scheme base on simple protograph structured codes," in *Proc. Int. Symp. Commun. and Inf. Technol.*, Oct. 2012, pp. 65–69.

[118] H. Wu, J. He, L. Xu, and L. Wang, "Joint source-channel coding based on P-LDPC codes for radiography images transmission," in *Proc. Int. Conf. Trust, Security, and Privacy in Comput. and Commun.*, Jun. 2012, pp. 2035–2039.

[119] L. Xu, H. Wu, J. He, and L. Wang, "Unequal error protection for radiography image transmission using protograph double LDPC codes," in *Proc. IEEE Wireless Telecommun. Symp. (WTS)*, Apr. 2013, pp. 1–5.

[120] H. Wu, L. Wang, S. Hong, and J. He, "Performance of joint source-channel coding based on protograph LDPC codes over Rayleigh fading channels," *IEEE Commun. Lett.*, vol. 18, no. 4, pp. 652–655, Apr. 2014.

[121] P. Chen and L. Wang, "A serial joint channel and physical layer network decoding in two-way relay networks," *IEEE Commun. Lett.*, vol. 16, no. 6, pp. 769–772, Jun. 2012.

[122] P. Chen, Y. Fang, L. Wang, and F. C. M. Lau, "Decoding generalized joint channel coding and physical network coding in the LLR domain," *IEEE Signal Process. Lett.*, vol. 20, no. 2, pp. 121–124, Feb. 2013.

[123] Y. Fang, L. Wang, K.-K. Wong, and K.-F. Tong, "Performance of joint channel and physical network coding based on Alamouti STBC," in *Proc. IEEE Int. Conf. Ultra-Wideband (ICUWB)*, Sept. 2013, pp. 243–248.

[124] K. Andrews, S. Dolinar, D. Divsalar, and J. Thorpe, "Design of low-density parity-check (LDPC) codes for deep-space applications," in *Proc. IPN Progress Report*, Nov. 2004, pp. 1–14.

[125] H. El Gamal, G. Caire, and M. Damen, "The MIMO ARQ channel: Diversity-multiplexing-delay tradeoff," *IEEE Trans. Inf. Theory*, vol. 52, no. 8, pp. 3601–3621, Aug. 2006.

[126] B. Zhao and M. Valenti, "Practical relay networks: a generalization of hybrid-ARQ," *IEEE J. Sel. Areas Commun.*, vol. 23, no. 1, pp. 7–18, Jan. 2005.

[127] H. Chen, R. Maunder, and L. Hanzo, "A survey and tutorial on low-complexity turbo coding techniques and a holistic hybrid ARQ design example," *IEEE Commun. Surveys & Tutorials*, vol. 15, no. 4, pp. 1546–1566, Fourth Quarter 2013.

[128] A. Sendonaris, E. Erkip, and B. Aazhang, "User cooperation diversity–Part I: System description," *IEEE Trans. Commun.*, vol. 51, no. 11, pp. 1927–1938, Nov. 2003.

[129] T. Cover and A. Gamal, "Capacity theorems for the relay channel," *IEEE Trans. Inf. Theory*, vol. 25, no. 5, pp. 572–584, Sept. 1979.

[130] P. Razaghi and W. Yu, "Bilayer low-density parity-check codes for decode-and-forward in relay channels," *IEEE Trans. Inf. Theory*, vol. 53, no. 10, pp. 3723–3739, Oct. 2007.

[131] T. Eng and L. B. Milstein, "Coherent DS-CDMA performance in Nakagami multipath fading," *IEEE Trans. Commun.*, vol. 43, no. 234, pp. 1134–1143, Feb. 1995.

[132] Y. Lee and M. H. Tsai, "Performance of decode-and-forward cooperative communications over Nakagami-m fading channels," *IEEE Trans. Veh. Technol.*, vol. 58, no. 3, pp. 1218–1228, Mar. 2009.

[133] A. Goldsmith, *Wireless Communications*. New York, NY, USA: Cambridge University Press, 2005.

[134] F. Lehmann and G. Maggio, "Analysis of the iterative decoding of LDPC and product codes using the Gaussian approximation," *IEEE Trans. Inf. Theory*, vol. 49, no. 11, pp. 2993–3000, Nov. 2003.

[135] B. S. Tan, K. H. Li, and K. Teh, "Performance analysis of LDPC codes with maximum-ratio combining cascaded with selection combining over Nakagami-m fading," *IEEE Trans. Wireless Commun.*, vol. 10, no. 6, pp. 1886–1894, Jun. 2011.

[136] E. Biglieri, J. Proakis, and S. Shamai, "Fading channels: Information-theoretic and communications aspects," *IEEE Trans. Inf. Theory*, vol. 44, no. 6, pp. 2619–2692, Oct. 1998.

[137] J. Boutros, A. Guillen i Fabregas, E. Biglieri, and G. Zemor, "Low-density parity-check codes for nonergodic block-fading channels," *IEEE Trans. Inf. Theory*, vol. 56, no. 9, pp. 4286–4300, Sept. 2010.

[138] A. Guillen i Fabregas and G. Caire, "Coded modulation in the block-fading channel: coding theorems and code construction," *IEEE Trans. Inf. Theory*, vol. 52, no. 1, pp. 91–114, Jan. 2006.

[139] J. Laneman, D. Tse, and G. W. Wornell, "Cooperative diversity in wireless networks: Efficient protocols and outage behavior," *IEEE Trans. Inf. Theory*, vol. 50, no. 12, pp. 3062–3080, Dec. 2004.

[140] T. Hunter, S. Sanayei, and A. Nosratinia, "Outage analysis of coded cooperation," *IEEE Trans. Inf. Theory*, vol. 52, no. 2, pp. 375–391, Feb. 2006.

[141] W. Ryan, "Performance of high rate turbo codes on a PR4-equalized magnetic recording channel," in *Proc. IEEE Int. Conf. Commun. (ICC)*, vol. 2, Jun. 1998, pp. 947–951.

[142] L. Bahl, J. Cocke, F. Jelinek, and J. Raviv, "Optimal decoding of linear codes for minimizing symbol error rate," *IEEE Trans. Inf. Theory*, vol. 20, no. 2, pp. 284–287, Mar. 1974.

[143] J. Li, K. Narayanan, E. Kurtas, and C. Georghiades, "On the performance of high-rate TPC/SPC codes and LDPC codes over partial response channels," *IEEE Trans. Commun.*, vol. 50, no. 5, pp. 723–734, May 2002.

[144] A. Kavcic, X. Ma, and M. Mitzenmacher, "Binary intersymbol interference channels: Gallager codes, density evolution, and code performance bounds," *IEEE Trans. Inf. Theory*, vol. 49, no. 7, pp. 1636–1652, Jul. 2003.

[145] H. Hemmati, *Deep Space Optical Communications*. New York, NY, USA: John Wiley & Sons, 2006.

[146] M. Barsoum, B. Moision, M. Fitz, D. Divsalar, and J. Hamkins, "EXIT function aided design of iteratively decodable codes for the Poisson PPM channel," *IEEE Trans. Commun.*, vol. 58, no. 12, pp. 3573–3582, Dec. 2010.

[147] D. Divsalar, S. Dolinar, J. Thorpe, and C. Jones, "Constructing LDPC codes from simple loop-free encoding modules," in *Proc. IEEE Int. Conf. Commun. (ICC)*, vol. 1, May 2005, pp. 658–662.

[148] S. Vembu, S. Verdu, and Y. Steinberg, "The source-channel separation theorem revisited," *IEEE Trans. Inf. Theory*, vol. 41, no. 1, pp. 44–54, Jan. 1995.

[149] M. Fresia, F. Perez-Cruz, and H. Poor, "Optimized concatenated LDPC codes for joint source-channel coding," in *Proc. IEEE Int. Symp. Inf. Theory (ISIT)*, Jun. 2009, pp. 2131–2135.

[150] M. Fresia, F. Perez-Cruz, H. V. Poor, and S. Verdu, "Joint source and channel coding," *IEEE Signal Process. Mag.*, vol. 27, no. 6, pp. 104–113, Nov. 2010.

[151] S. Zhang, S.-C. Liew, , and P. Lam, "Hot topic: physical layer network coding," in *Proc. MobiCom'06*, Sept. 2006, pp. 358–365.

[152] P. Qin, B. Dai, B. Huang, G. Xu, and K. Wu, "A survey on network tomography with network coding," *IEEE Commun. Surveys & Tutorials*, vol. 16, no. 4, pp. 1981–1995, Fourth Quarter 2014.

[153] S. Zhang and S.-C. Liew, "Channel coding and decoding in a relay system operated with physical-layer network coding," *IEEE J. Sel. Areas Commun.*, vol. 27, no. 5, pp. 788–796, Oct. 2009.

[154] Y. Lang and D. Wubben, "Generalized joint channel coding and physical network coding for two-way relay systems," in *Proc. IEEE Veh. Technol. Conf. (VTC)*, May 2010, pp. 1–5.

[155] D. Wubben and Y. Lang, "Generalized sum-product algorithm for joint channel decoding and physical-layer network coding in two-way relay systems," in *Proc. IEEE Global Telecommun. Conf. (GLOBECOM)*, Dec. 2010, pp. 1–5.

[156] T. Huang, T. Yang, J. Yuan, and I. Land, "Design of irregular repeat-accumulate coded physical-layer network coding for Gaussian two-way relay channels," *IEEE Trans. Commun.*, vol. 61, no. 3, pp. 897–909, Mar. 2013.

[157] Y. Ng, K. Cai, B. Kumar, S. Zhang, and T. C. Chong, "Modeling and two-dimensional equalization for bit-patterned media channels with media noise," *IEEE Trans. Magn.*, vol. 45, no. 10, pp. 3535–3538, Oct. 2009.

[158] L. Kong, Y. L. Guan, J. Zheng, G. Han, K. Cai, and K.-S. Chan, "EXIT-chart-based LDPC code design for 2D ISI channels," *IEEE Trans. Magn.*, vol. 49, no. 6, pp. 2823–2826, Jun. 2013.

[159] G. Han, Y. L. Guan, K. Cai, and K. S. Chan, "Asymmetric iterative multi-track detection for 2-D non-binary LDPC-coded magnetic recording," *IEEE Trans. Magn.*, vol. 49, no. 10, pp. 5215–5221, Oct. 2013.

[160] I. B. Djordjevic and T. Wang, "Multiple component codes based generalized LDPC codes for high-speed optical transport," *Opt. Express*, vol. 22, no. 14, pp. 16 694–16 705, Jul. 2014.

[161] A. Shokrollahi, "Raptor codes," *IEEE Trans. Inf. Theory*, vol. 52, no. 6, pp. 2551–2567, Jun. 2006.